Life Sciences 351 (2024) 122810

Contents lists available at ScienceDirect

Life Sciences

journal homepage: www.elsevier.com/locate/lifescie

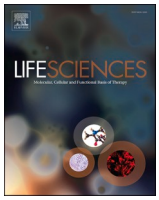

Proteomic analysis of endothelial cells and extracellular vesicles in response to indoxyl sulfate: Mechanisms of endothelial dysfunction in chronic kidney disease

Andrea Figuer [a,b], Fátima M. Santos [c,d], Sergio Ciordia [d], Gemma Valera [e,f], Beatriz Martín-Jouve [g], Juan Pablo Hernández-Fonseca [g], Guillermo Bodega [h], Noemí Ceprián [e], Rafael Ramírez [a,b], Julia Carracedo [e,f,*,1], Matilde Alique [a,b,**,1]

[a] Departamento de Biología de Sistemas, Universidad de Alcalá, 28871 Alcala de Henares, Madrid, Spain
[b] Instituto Ramón y Cajal de Investigación Sanitaria (IRYCIS), 28034 Madrid, Spain
[c] Cellular Biology in Renal Diseases Laboratory, IIS-Fundación Jiménez Díaz-Universidad Autónoma Madrid, 28040 Madrid, Spain
[d] Functional Proteomics Laboratory, Centro Nacional de Biotecnología, CSIC, Calle Darwin 3, Campus de Cantoblanco, 28049 Madrid, Spain
[e] Departamento de Genética, Fisiología y Microbiología, Universidad Complutense, 28040 Madrid, Spain
[f] Instituto de Investigación Sanitaria Hospital 12 de Octubre (imas12), 28040 Madrid, Spain
[g] Electron Microscopy Unit, Centro Nacional de Biotecnología, CSIC, Calle Darwin 3, Campus de Cantoblanco, 28049 Madrid, Spain
[h] Departamento de Biomedicina y Biotecnología, Universidad de Alcalá, 28871 Alcala de Henares, Madrid, Spain

ARTICLE INFO

Keywords:
Cardiovascular disease
Chronic kidney disease
Endothelial dysfunction
Extracellular vesicles
Indoxyl sulfate
Proteomics

ABSTRACT

Aims: Cardiovascular pathology is the main cause of death in chronic kidney disease (CKD) patients. CKD is associated with the accumulation of uremic toxins in the bloodstream, and indoxyl sulfate (IS) is one of the most abundant uremic toxins found in the blood of CKD patients. We conducted an in vitro study to assess the mechanisms underlying the IS-induced endothelial dysfunction that could lead to cardiovascular diseases. We also studied their extracellular vesicles (EVs) owing to their capacity to act as messengers that transmit signals through their cargo.

Main methods: EVs were characterized by nanoparticle tracking analysis, transmission electron microscopy, flow cytometry, and tetraspanin expression. Cell lysates and isolated EVs were analyzed using liquid chromatography coupled with mass spectrometry, followed by Gene Set Enrichment Analysis to identify the altered pathways.

Key findings: Proteomic analysis of endothelial cells revealed that IS causes an increase in proteins related to adipogenesis, inflammation, and xenobiotic metabolism and a decrease in proliferation. Extracellular matrix elements, as well as proteins associated with myogenesis, response to UV irradiation, and inflammation, were found to be downregulated in IS-treated EVs. Fatty acid metabolism was also found to be increased along with adipogenesis and inflammation observed in cells.

Significance: The treatment of endothelial cells with IS increased the expression of proteins related to adipogenesis, inflammation, and xenobiotic metabolism and was less associated with proliferation. Furthermore, EVs from cells treated with IS may mediate endothelial dysfunction, since they present fewer extracellular matrix elements, myogenesis, inflammatory factors, and proteins downregulated in response to UV radiation.

Abbreviations: CKD, chronic kidney disease; EVs, extracellular vesicles; FC, flow cytometry; FDR, false discovery rate; GSEA, Gene Set Enrichment Analysis; HUVECs, human umbilical vein endothelial cells; IS, indoxyl sulfate; NTA, nanoparticle tracking analysis; RT-qPCR, reverse transcription-quantitative polymerase chain reaction; SASP, senescent associated secretory phenotype; SIPS, stress-induced premature senescence; TEM, transmission electron microscopy; UV, ultraviolet.

* Correspondence to: J. Carracedo, Departamento de Genética, Fisiología y Microbiología, Universidad Complutense, 28040 Madrid, Spain.
** Correspondence to: M. Alique, Departamento de Biología de Sistemas, Universidad de Alcalá, 28871 Alcala de Henares, Madrid, Spain.
E-mail addresses: julcar01@ucm.es (J. Carracedo), matilde.alique@uah.es (M. Alique).
[1] Co-senior authors.

https://doi.org/10.1016/j.lfs.2024.122810
Received 3 April 2024; Received in revised form 19 May 2024; Accepted 4 June 2024
Available online 11 June 2024

1. Introduction

Chronic kidney disease (CKD) presents as a reduced glomerular filtration rate of 60 mL/min/1.73 m^2 or evident structural kidney damage for over three months [1]. It is estimated to become the 5th most common cause of death by 2040, affecting >10 % of the population worldwide [2], owing to the aging of the world population [3].

CKD causes the accumulation of uremic toxins in the blood. Uremic toxins are associated with proteins, making their filtration by dialysis more difficult [4]. Uremic toxins are in contact with endothelial cells and induce oxidative stress and low-level systemic inflammation [5]. This phenomenon leads to endothelial dysfunction, characterized by the loss of endothelial barrier function, endothelial senescence, vasoconstriction, acquisition of a pro-inflammatory and pro-thrombotic state, and arterial remodeling. Endothelial dysfunction increases the risk of cardiovascular diseases (CVD), such as atherosclerosis and vascular calcification, which explains why patients with CKD have a higher risk of CVD than the general population [6]. These diseases are predominant in the elderly, which explains why CKD produces premature aging [7–9]. Physiological aging is caused by cellular senescence, mitochondrial dysfunction, loss of proteostasis, and altered intercellular communication [10], which has been observed in patients with CKD. Related to aging, there is a release of chemokines, pro-inflammatory cytokines, and proteases, which are known as senescence-associated secretory phenotypes (SASP) [11,12]. SASP factors are present in the plasma of patients with CKD [13]. Other authors have defined the phenotype found in patients with CKD as stress-induced premature senescence (SIPS) to differentiate between physiological aging and aging induced by environmental factors [14].

Indoxyl sulfate (IS) is one of the most abundant uremic toxins [15]. IS causes premature aging of the endothelium, and is associated with atherosclerotic plaque formation [16,17]. Moreover, IS is correlated with mortality and comorbidities such as vascular calcification, stiffness, and congestive heart failure in patients with end-stage renal disease [18].

Extracellular vesicles (EVs) also participate in the pathophysiology of CKD. EVs are secreted by all cell types [12] and act as intercellular communication systems that transport lipids, proteins, and microRNAs to modulate cellular functions [9]. Multiple pathologies have been associated with increased EV secretion [19]. Therefore, EV cargo can predict its implications in pathophysiology. For example, in cancer, EVs potentiate metastasis, angiogenesis, coagulation, metabolic reprogramming, and immunosuppression [20]. In CKD, patients undergoing hemodialysis have a higher number of EVs; however, high EV levels can also be linked to other associated diseases such as hypertension, diabetes mellitus, and coronary artery disease [21]. Moreover, an in vitro study demonstrated that endothelial cells treated with IS produce pro-calcifying EVs [22]. EVs could be promising predictive and diagnostic markers of diseases because they carry information from less accessible cell types such as endothelial cells. Furthermore, they can be considered as potential therapeutic targets, considering their modulatory function and role in maintaining cardiovascular homeostasis [23,24].

This study aimed to elucidate the mechanism by which uremic toxins such as IS mediate endothelial injury. Through proteomic analyses, we characterized changes in endothelial cells and EV cargo produced by IS. To the best of our knowledge, this research represents the first study to identify novel biomarkers that could prove beneficial as diagnostic, prognostic, and therapeutic tools for CVD associated with CKD.

2. Experimental procedures

2.1. Cell culture and indoxyl sulfate treatment

Human umbilical vein endothelial cells (HUVECs; CC-2517, lot number 323352; Lonza Bioscience, Walkersville, MD, USA) were cultured in endothelial basal medium (EBM; CC-3121; Lonza Bioscience) supplemented with EGM SingleQuots (CC-4133; Lonza Bioscience) and 10 % heat-inactivated fetal bovine serum (FBS; F7524; Sigma-Aldrich, St. Louis, MO, USA). The cultures were maintained at 37 °C under 5 % CO_2 and 95 % humidity. Experiments involving HUVECs were performed using cells passaged <9 times. Cell passages were performed using trypsin-EDTA solution diluted in phosphate-buffered saline (PBS; T4174; Sigma-Aldrich). IS (I3875; Sigma-Aldrich) was diluted in DMSO to a concentration of 0.5 M and stored at −20 °C. IS was added to the culture medium when the cells reached the desired confluence at a final concentration of 250 μM, and incubated for 24 h. This concentration of IS is clinically relevant because it is similar to that observed in patients with advanced CKD [25,26] and is commonly used to induce phenotypic changes in HUVECs [22,27] without cytotoxicity [28].

2.2. Extracellular vesicle isolation

EVs were isolated from culture media as previously described [22]. Briefly, culture media from the controls and cells treated with IS were obtained and centrifuged (Centrifuge 5702R; Eppendorf, Hamburg, Germany) for 15 min at 1400 ×*g* to eliminate cell debris. The supernatants were centrifuged for 30 min at 20,000 ×*g* (Centrifuge 5427R; Eppendorf). The resulting pellet, corresponding to the EVs, was washed twice with PBS 1× filtrated through 0.2-μm sterile filters (431,219; Corning Life Sciences, Corning, NY, USA).

2.3. Characterization of the extracellular vesicles

After isolation, EVs were characterized according to the International Society for Extracellular Vesicles (ISEV2023) guidelines (MISEV2023) [29]. Specifically, EVs were imaged and measured using transmission electron microscopy (TEM), and the quantity, size, and expression of tetraspanins were determined using flow cytometry. These results were corroborated by nanoparticle tracking analysis (NTA) results.

2.3.1. Extracellular vesicle imaging and characterization by transmission electron microscopy

Pools of EVs from IS-treated endothelial cells and controls ($n = 4$) were resuspended in filtered PBS. For negative staining, glow discharge was performed on carbon-coated collodion 400 mesh nickel grids (Glider). Each sample (15 μL) was then adsorbed onto a grid for 2 min. The grids were subsequently washed with two drops of Milli Q water, stained with 2 % aqueous uranyl acetate (Electron Microscopy Sciences) for 1 min, and left to dry at room temperature. The grids were observed using a JEOL JEM 1400 flash electron microscope (operating at 100KV). Micrographs were obtained with a Gatan One View digital camera at various magnifications. EVs were measured using DigitalMicrograph software (version 3.51.3720.0; Gatan Inc., Pleasanton, CA, USA), considering the exterior and interior measurement diameters of the vesicles ($n = 20$) for each sample ($n = 8$). Measurements were performed in vesicles, in which both diameters were easily visible. Data are expressed as mean ± standard deviation (SD) and were analyzed using an unpaired *t*-test.

2.3.2. Nanoparticle tracking analysis

The size distribution of the EV samples was assessed using NTA. We tested our isolated samples diluted in 1 mL of 0.2-μm filtered PBS using a NanoSight Pro Nanoparticle Tracking Analyzer (Malvern Panalytical, Malvern, UK). The particles were tracked using a 488 nm laser for 11.54 s to assess their Brownian motion. This process was repeated five times, and five videos were acquired for each sample. NS XPLORER (v1.0.8641.14) software was used to analyze the movement and calculate the size distribution profiles and concentration measurements.

2.3.3. Western blotting of extracellular vesicles

Western blotting for EVs was performed to assess the presence of EV

markers. An exosome panel (ab275018; Abcam, Cambridge, UK) containing anti-TSG-101, anti-HSP70, anti-CD9, and anti-CD63 antibodies was used. Anti-TSG-101 and anti-HSP70 were incubated under reducing conditions, whereas the rest were used under non-reducing conditions. The EV samples were lysed and centrifuged to obtain proteins, which were measured in duplicate using the BCA assay method. Electrophoresis was performed in Novex WedgeWells 4–20 % Tris-glycine gels (Thermo Fisher Scientific, Waltham, MA, USA) with 5 μg of total protein dissolved in 10 μL of the corresponding charge buffer and heated at 95 °C for 1 min. After electrophoresis, the samples were transferred to a Trans-Blot Turbo Transfer System (BioRad Laboratories, Hercules, CA, USA), stained with Ponceau Red, and washed with distilled water. The membrane was blocked with PBS-Tween 0.1 % 5 % bovine serum albumin (BSA) for 1 h at room temperature. Subsequently, the membranes were incubated overnight with primary antibodies (diluted 1:1000 in PBS-T and 1 % BSA) at 4 °C. Thereafter, the membranes were washed with PBS-T and incubated with the corresponding secondary antibody at 1:5000 dilution for 1 h at room temperature. Finally, membranes were washed with SuperSignal (Thermo Fisher Scientific) for protein detection.

2.3.4. Extracellular vesicle quantification flow cytometry

The EVs were resuspended in PBS 1× and incubated with 1 μM CFSE for 45 min at 37 °C and 5 % CO_2. The samples were then analyzed using a MACSQuant10 Analyzer and MACSQuantify software (version 2.13.0; Miltenyi Biotec, Bergisch Gladbach, Germany).

To quantify tetraspanin expression and size, EVs were incubated for 1 h at room temperature with anti-CD9-488/anti-CD81-555/anti-CD63-647 (Leprechaun kit; Unchained Labs, Pleasanton, CA, USA), followed by EV labeling with 25 μM Tag-it Violet (#425101, BioLegend, San Diego, CA, USA) for 90 min at 37 °C to differentiate the EVs from noise. Subsequently, the samples were analyzed by flow cytometry using a CytoFLEX S Flow Cytometer (Beckman Coulter, Brea, CA, USA), and FCM Pass software (NIH, Bethesda, MD, USA) was used to estimate EV size based on their refractive index for size calibration. The detailed methodology can be found in Supplementary Data 1, including a report structured according to the guidelines [30].

2.3.5. Extracellular vesicle protein cargo quantification

To determine the total amount of protein per EV, 280,000 cells were seeded and treated with IS for 24 h on the following day. Total EVs were isolated from the control and IS-treated groups and a portion of their volume was used for quantification by flow cytometry. Protein concentration was quantified using the Pierce™ BCA Protein Assay Kit (23,225, Thermo Fisher Scientific) with the Quick Start BSA Standard Set (500-0207, BioRad Laboratories) as a standard. Absorbance was measured using a plate reader (FLUOstar Omega, BMG LABTECH, Ortenberg, Germany). The protein cargo results were standardized by the number of endothelial cells from which they were released after quantification at the final time point. The results are expressed per million cells. GraphPad Prism 8.0.2 (GraphPad Software, La Jolla, CA, USA) was used for graphical representation and statistical analysis (paired *t*-test).

2.4. Preparation of samples for proteomics analysis

HUVECs and HUVEC-derived EVs were pooled and preserved as dry pellets at −20 °C ($n = 5$). The samples were lysed with 400 μL and 150 μL of 5 % sodium dodecyl sulfate and 25 mM triethylammonium bicarbonate supplemented with 5 mM tris(2-carboxyethyl) phosphine and 10 mM chloroacetamide. The lysates were sonicated using an ultrasonic processor UP50H (Hielscher Ultrasonics, Teltow, Germany) for 1 min on ice (0.5 cycles, 100 % amplitude) and incubated at 56 °C for 30 min. Protein lysates were centrifuged at 18,400 ×*g* for 10 min and the supernatant was transferred to a new tube. Total protein was measured using the PIERCE 660 nm reagent (Thermo Fisher Scientific) supplemented with an Ionic Detergent Compatibility Reagent (Thermo Fisher Scientific). Protein digestion was performed using S-Trap columns (Protifi, Farmingdale, NY, USA) according to the manufacturer's instructions [31]. Briefly, 20 μg of each sample was digested overnight at 37 °C using a trypsin:protein ratio of 1:15. Tryptic peptides were cleaned using in-house made Stage-Tips prepared from Octadecyl C18 Solid-phase Extraction Disks (Empore™, 66,883-U), as previously described [32]. The eluted peptides were dried in a speed vacuum and stored at −20 °C until further processing.

2.5. Analysis by liquid chromatography coupled to mass spectrometry

Each sample was quantified by fluorimetry (QuBit; Thermo Fisher Scientific), and 1 μg was individually analyzed by nanoliquid chromatography coupled with electrospray ionization tandem mass spectrometry (nanoLC-ESI-MS/MS) using an Ultimate 3000 nano HPLC system (Thermo Fisher Scientific) coupled online to an Orbitrap Exploris™ 240 mass spectrometer (Thermo Fisher Scientific). Samples were loaded on a 50 cm × 75 μm Easy-spray PepMap C18 analytical column (Thermo Fisher Scientific) at 45 °C and separated at a flow rate of 250 nL/min using a 120-min gradient ranging from 2 to 95 % mobile phase B (80 % acetonitrile in 0.1 % FA). Two 40-min blank samples were systematically run between samples to avoid carry-over. Data acquisition was performed using a data-dependent top-20 method in the full-scan positive mode and scanning at 375–1200 *m/z*. MS1scans were acquired at an Orbitrap resolution of 60,000 at *m/z* 200, with a normalized automatic gain control (AGC) target of 300 %, a radio frequency lens of 80 %, and an automatic maximum injection time (IT). The most intense ions from each MS1 scan were selected and fragmented at a higher-energy collisional dissociation (HCD) of 30 %. The resolution of the HCD spectra was set to 15,000 at *m/z* 200, with a normalized AGC target of 50 % and an automatic maximum IT. The precursors were isolated at an isolation window of 2 *m/z* and an exclusion duration of 45 s. Precursor ions with charge states ranging from 2^+ to 5^+ were included.

2.6. Mass spectrometry data analysis

Mass spectrometry data were processed using Proteome Discoverer (v2.5.0.400; Thermo Fisher Scientific) as previously described [33–35]. Database searches were performed using four search engines [Mascot (v2.7.0), MsAmanda (v2.4.0), MsFragger (v3.1.1), and Sequest HT] against the *Homo Sapiens* UniProtKB database (February 19, 2021; 20,378 sequences) containing the most common laboratory contaminants (a cRAP database with 69 sequences). The search parameters were set as follows: cysteine carbamidomethylation (+57.021464 Da), methionine oxidation (M) (+15.994915 Da), *N*-terminal acetylation (+42.010565 Da), and Gln → pyro-Glu (−17.026549 Da) as variable modifications. The precursor and fragment mass tolerances were set to 10 and 0.02 Da, respectively, and trypsin/P was selected as the protease with a maximum of two missed cleavage sites. The false discovery rate (FDR) for proteins, peptides, and peptide-spectral matched peptides was maintained at 1 %. Quantitation was also performed in the Proteome Discoverer using the "Minora Feature Detector" processing method and the "Feature Mapper" and "Precursor Ions Quantifier" nodes in the consensus step. The "Feature Mapper" node was applied using chromatographic retention time alignment with a maximum shift of 10 min and signal-to-noise threshold of 5. Quantitation and normalization were performed using the following parameters: unique + razor peptides, precursor abundance based on intensity without imputation, and normalization mode based on total peptide amount. This normalization mode was performed by dividing the summed abundances for a specific peptide group in each sample by the normalization factor (the sum of all calculated peptide intensities for all samples). Protein abundance was calculated by summing the sample abundance of the connected peptide groups. The mass spectrometry proteomics data were deposited in the ProteomeXchange Consortium via the PRIDE [36] partner repository

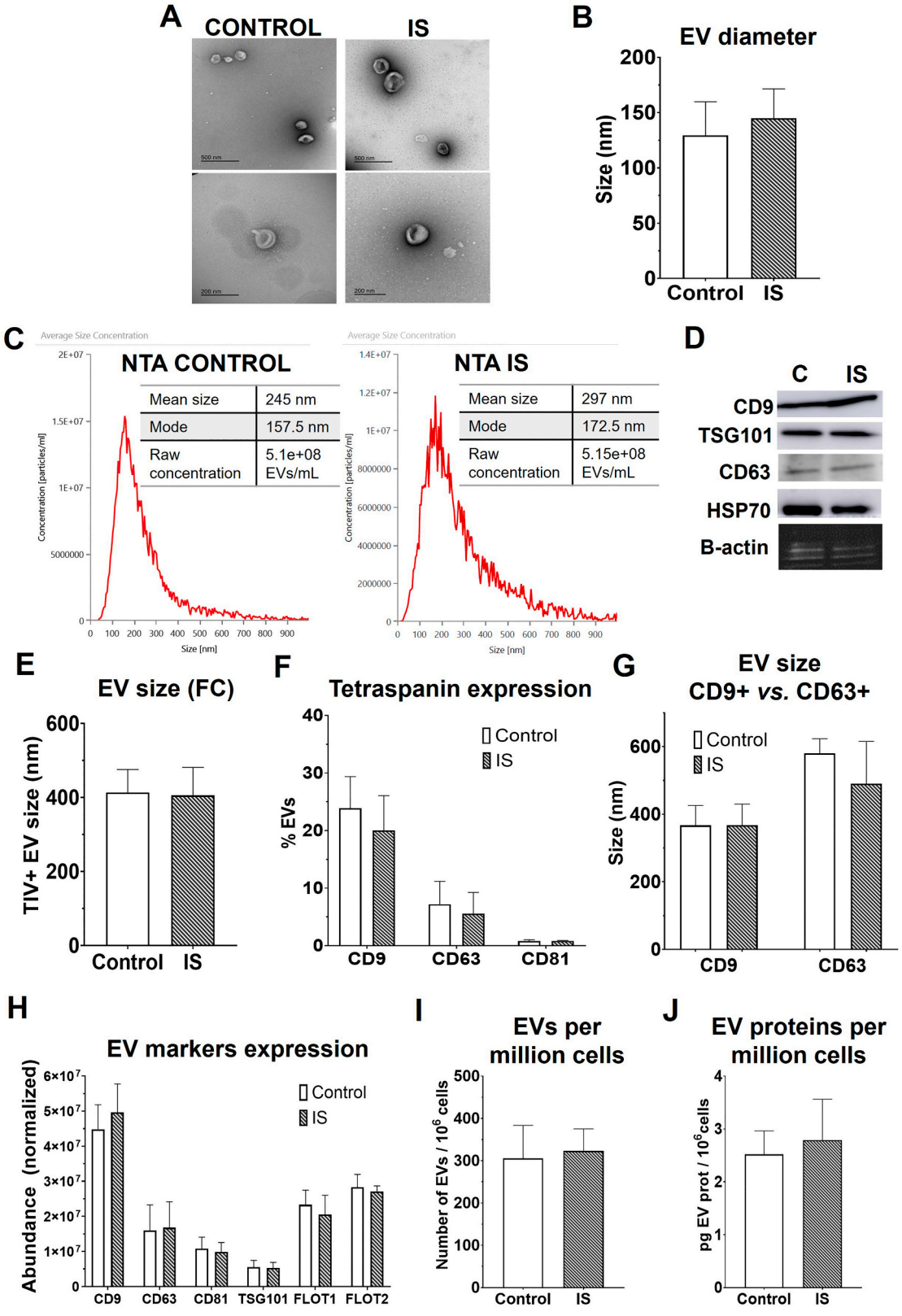

Fig. 1. Characterization of endothelial extracellular vesicles (EVs). A) Representative EVs observed by transmission electron microscopy and B) diameters obtained as the mean value of 20 EVs in four samples per condition ($n = 4$). C) Size distribution was characterized using nanoparticle tracking analysis. D) Expression of different EV markers was evaluated using western blotting ($n = 3$). E) The relative size of the EVs (stained with Tag-it Violet) was measured by flow cytometry ($n = 3$), F), wherein we also measured tetraspanin expression and G) size per marker. H) Tetraspanin expression determined by mass spectrophotometry ($n = 5$). I) Production of EVs per million cells and J) Quantification of protein cargo. Data are presented as the mean ± SD.

with the dataset identifiers PXD050628 and https://doi.org/10.6019/PXD050628. Pairwise-based ratios were calculated, and a *t*-test background-based statistical test was performed to compare treated cells with untreated cells/EVs. A *p*-value ≤ 0.05 was adjusted using the Benjamini–Hochberg method, and a fold change (FC) of at least 25 % was set to determine the differentially enriched proteins. Volcano plots were generated using the EnhancedVolcano R package [37]. Gene Set Enrichment Analysis (GSEA) [38] was performed using gene set permutations ($n = 1000$) for the assessment of significance, signal-to-noise metrics for ranking genes, and hallmark gene set collections defined by the Molecular Signatures Database [39]. Known functional interactions among the relevant genes were obtained using STRING [40]. Cytoscape software was used to integrate and visualize the network data [41].

2.7. Proliferation assay

For proliferation testing, we used a 5-bromo-2′-deoxyuridine (BrdU) Cell Proliferation ELISA Kit (colorimetric) (AB126556; Abcam) according to the manufacturer's instructions. A total of 2000 cells per well were cultured in triplicate in a 96-well plate. The following day, some cells were treated with IS for 24 h. BrdU was added to all wells, except for the negative control, 4 h before treatment finalization. Absorbance was measured using a plate reader (FLUOstar Omega, BMG LABTECH). The results are expressed as a ratio compared with the control absorbance (OD IS/OD control).

2.8. Reverse transcription-quantitative polymerase chain reaction (RT q-PCR)

RNA was extracted from cells using a mirVana PARIS RNA and Native Protein Purification Kit (AM1556; Invitrogen, Carlsbad, CA, USA) according to the manufacturer's instructions. cDNA was synthesized using a High-Capacity cDNA Reverse Transcription Kit (REF: 4368814; Applied Biosystems, Waltham, MA, USA) with 2 μg of total RNA primed with random hexamer primers following the manufacturer's instructions. Real-time polymerase chain reaction (PCR) was performed using TaqMan Universal Master Mix II, no UNG (REF: 444040; Applied Biosystems), according to the manufacturer's protocol, on a QuantStudio™ 12 K Flex Real-Time PCR System with an AccuFill OpenArray™ block (Applied Biosystems). The assay ID used was: ICAM-1: Hs00164932_m1, MCP-1 (CCL2): Hs00234140_m1, IL-6: Hs00174131_m1. The data were normalized to HPRT1 (assay ID: Hs02800695_m1). The mRNA copy numbers were calculated for each sample using instrument software and the comparative threshold (Ct) value. Relative FC was determined using the $2-\Delta\Delta Ct$ method, with control HUVECs as the baseline, and normalized to HPRT1 expression.

2.9. Statistical analysis and graphical representation

Data representation and statistical analyses were performed using GraphPad Prism, version 8.0.2 (GraphPad Software). Normality was evaluated using the Kolmogorov–Smirnov test, followed by a paired *t*-test for values with a normal distribution and a Wilcoxon test for non-parametric data. The results are presented as mean ± standard deviation. Statistical significance was set at $p < 0.05$.

3. Results

3.1. Extracellular vesicles production and characterization

According to the ISEV guidelines, several methods were used to confirm whether the samples were isolated from the supernatants containing EVs. First, EVs were visualized using TEM (Fig. 1A; additional images are provided in Supplementary Fig. 1), showing no degradation or contamination. EVs have a well-defined shape with a homogeneous morphology and variable sizes (70–150 nm). Twenty vesicles per sample were measured (Fig. 1B), showing no differences between the IS-treated and control samples (0.145 ± 0.026 vs. 0.129 ± 0.031 μm). NTA also confirmed that the analyzed particles were compatible with EVs, with no apparent differences between conditions (Fig. 1C). The expression of tetraspanins (pan-EV markers) was measured using western blotting. Specifically, CD9, TSG101, CD63, and HSP70 were detected, but no differences were observed between the control and IS groups (Fig. 1D). In addition, EVs were measured using flow cytometry and compared with beads of known sizes; no differences were observed between the control and IS groups (Fig. 1E). The expression of the tetraspanins CD9, CD63, and CD81 was also assessed by flow cytometry (Fig. 1F). The majority of EVs were CD9+, followed by CD63+ and CD81+, and some exhibited double or triple expression (Supplementary Data 1). In addition, no significant differences in size were observed between the control and IS-treated groups when grouped by marker (Fig. 1G). The markers and other EVs were also measured by nanoLC-ESI-MS/MS (label-free experiment), but no significant differences were observed between the conditions, following the same abundance distribution of CD9, CD63, and CD81 as measured by flow cytometry (Fig. 1H).

After confirming the identity of our sample as EVs, we determined whether the release or amount of protein cargo had changed. The production of EVs per million endothelial cells was 323.2 ± 52.13 in the IS-treated group vs. 305.4 ± 78.08 in the controls, therefore, no significant differences were found (Fig. 1I). In addition, the protein cargo in the IS-treated vs. control groups (2.79 ± 0.77 vs. 2.52 ± 0.45 pg/million cells) did not differ (Fig. 1J). This indicated that treatment with IS did not induce changes in the number of EVs or the amount of proteins in the EVs after 24 h of treatment.

3.2. Proteomics analysis of endothelial cells revealed upregulation of proteins that participate in adipogenesis, inflammation, and xenobiotic metabolism

The protein profile of HUVECs was analyzed after treatment with IS to evaluate changes in protein expression. By analyzing these cells using label-free quantitative (LFQ) proteomics, 5871 proteins (5836 protein groups) were identified with high confidence (false discovery rate (FDR) confidence: *q*-value ≤ 1 %), and 5692 protein groups were quantified (Supplementary Table 1). Differential enrichment analyses revealed 82 differentially expressed proteins between IS-treated HUVECs and controls, of which 33 were up-regulated and 49 were down-regulated (Fig. 2A). These proteins were represented according to their statistical significance ($-\log_{10} p$-value) and fold change ($\log_2$) in a volcano plot (Fig. 2B). As seen in Table 1, GSEA identified three pathways upregulated after IS treatment (Fig. 2C): adipogenesis (Fig. 3), Tumor Necrosis Factor (TNF) signaling via NFκB (Fig. 4), and xenobiotic metabolism (Fig. 5). To confirm the activation of NFκB, we performed qPCR of some target genes of this nuclear factor (Fig. 4C), specifically ICAM-1 (adhesion molecule), MCP-1 (CCL2, a chemokine), and IL-6 (a pro-inflammatory cytokine), which were found to be overexpressed after IS treatment; all were related to endothelial dysfunction. We also explored >5000 gene sets related to inflammation using GSEA and selected their core enrichment proteins, which were expressed in a network (Fig. 4D). The core enrichment proteins of these altered functions (Table 1) were represented in a network (Fig. 2D), remarking CYP1A1, a consequence of the aryl hydrocarbon receptor (AhR) described in CKD [42], and PTGS2, also known as COX-2, whose activation is related to inflammation through eicosanoid production. In addition, the PI3K/AKT/mTOR pathway, which regulates cell survival, proliferation, and anabolic metabolism [43,44], was inhibited in endothelial cells after IS treatment. However, GSEA was inconclusive because even though the nominal *p*-value was significant, the FDR was high, indicating insufficient statistical evidence to confirm that the PI3K/AKT/mTOR pathway was inhibited. As this pathway is involved in regulating cell proliferation, a proliferation assay was performed, which revealed reduced cell proliferation following IS treatment

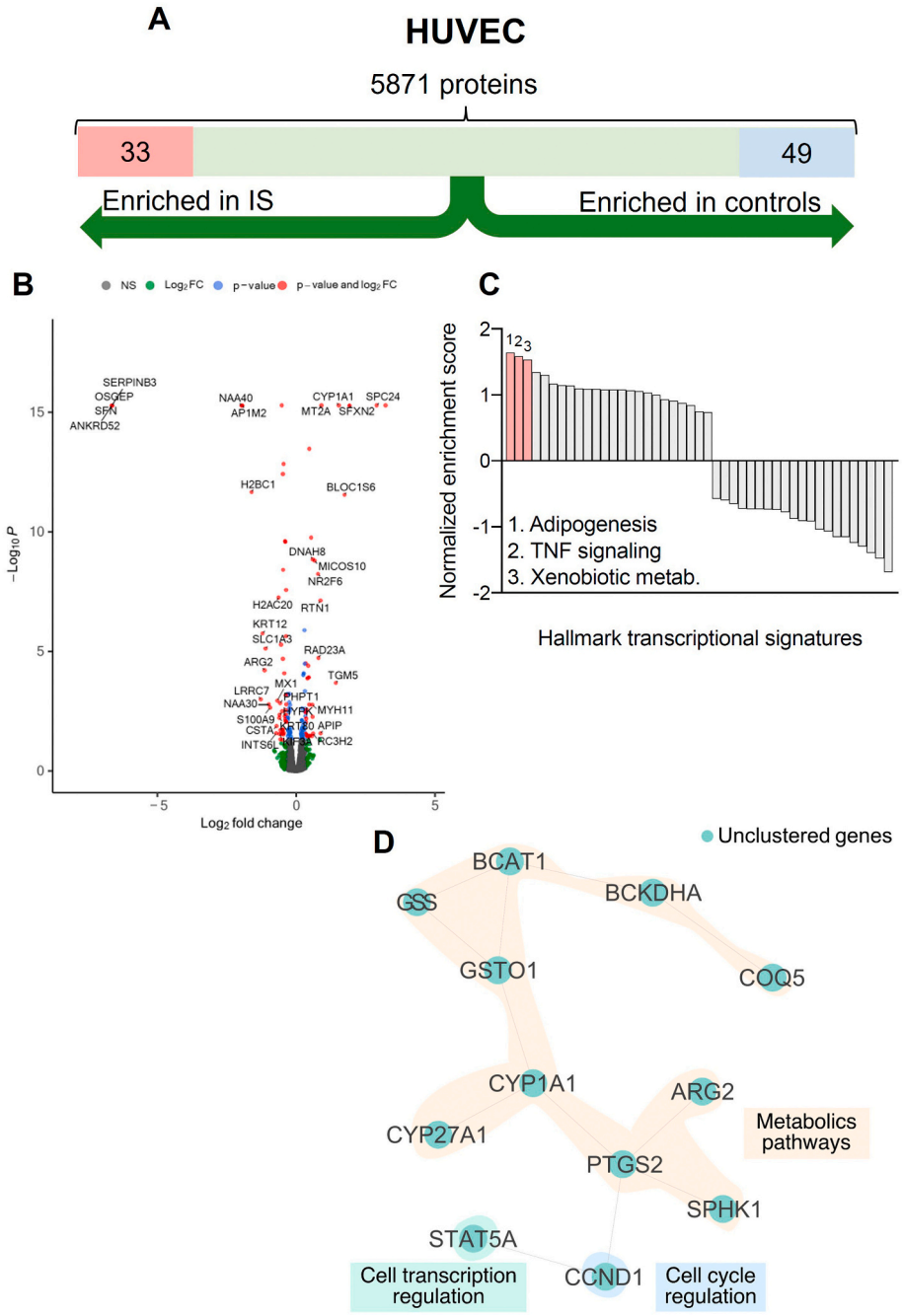

Fig. 2. Proteomic analysis of endothelial cells treated with indoxyl sulfate (IS) versus controls (IS versus C) ($n = 5$). A) A total of 5871 proteins with q-value ≤ 0.01 (False Discovery Rate) were identified, of which 49 were more abundant in the controls (blue) and 33 in the IS-treated (red) group. B) Volcano plot displaying the proteins quantified according to their statistical significance and fold-change (FC). Differentially expressed proteins between the IS-treated and control groups with an adjusted p-value < 0.05 (FDR) and log2 of least 25 % are colored in red, with the proteins showing upregulation represented on the right (log2 FC > 0) and downregulation on the left (log2 FC < 0). Proteins with no significant differences (gray), a $\log_2$ FC (fold change) of at least 25 % (green), and an adjusted p-value $<$ 0.05 (blue), are also shown. C) GSEA revealed three pathways upregulated by IS treatment (red). D) Protein-protein interaction network formed by the core enrichment proteins of the significant pathways (Table 1).

(Supplementary Fig. 2).

3.3. *Proteomics analysis of extracellular vesicles shows fewer extracellular matrix elements and fewer proteins related to myogenesis, cell cycle control, and inflammation*

To evaluate changes in EV protein cargo, an LFQ proteomic study of EVs released by endothelial cells after IS treatment was performed. A total of 3614 proteins (3546 protein groups) were identified with high confidence (FDR confidence: q-value $\leq$ 1 %), of which 3339 protein groups were quantified (Supplementary Table 1). After statistical analysis, 104 proteins were found differentially expressed between EVs secreted from HUVECs treated with IS and controls: 54 were upregulated and 50 were downregulated (IS-treated vs. control) (Fig. 6A). These proteins are represented in a volcano plot (Fig. 6B), considering their statistical significance ($\log_{10}$ p-value) and fold change (log2). To evaluate the effect of IS treatment on EV cargo, GSEA results (Fig. 6C) revealed the downregulation of proteins related to the extracellular

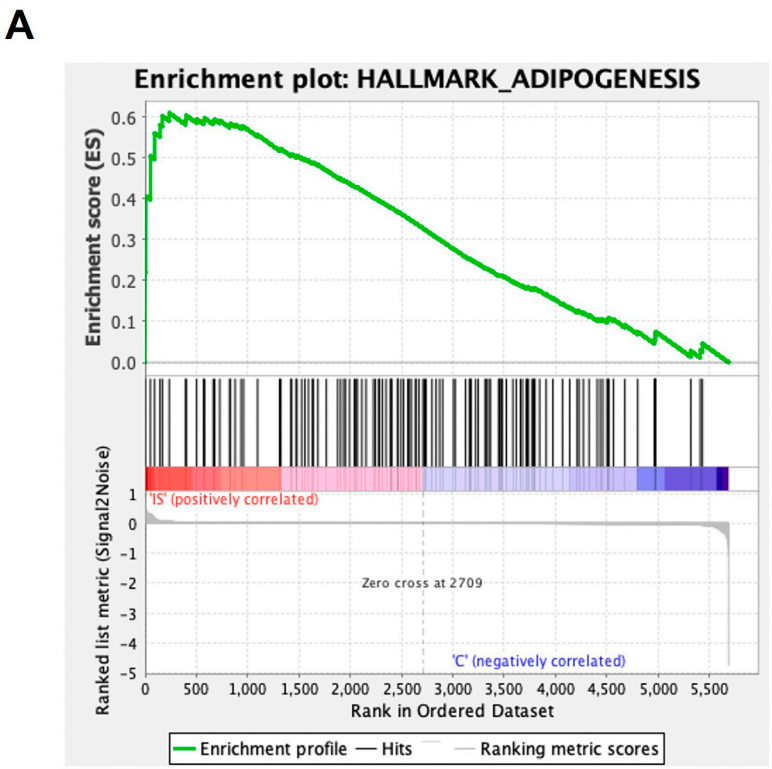

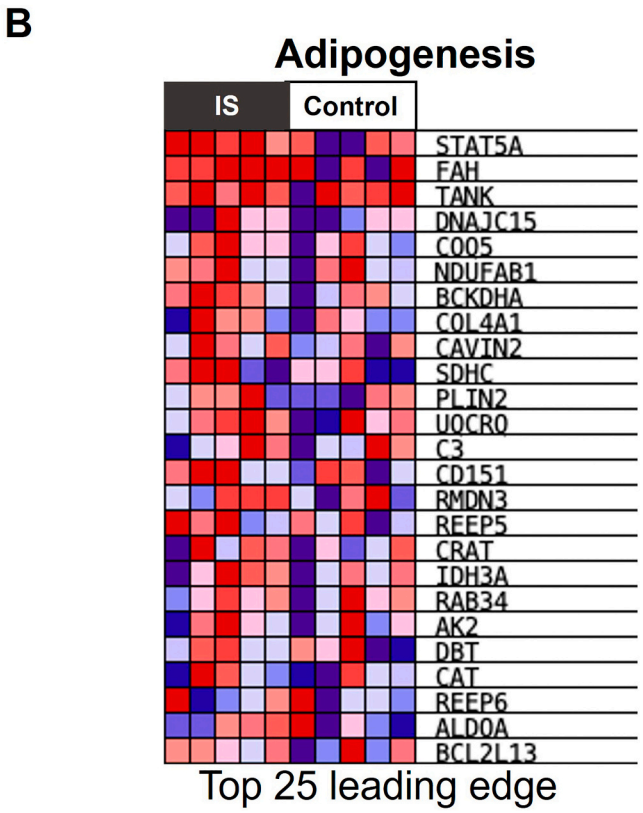

Fig. 3. GSEA revealed increased adipogenesis in indoxyl sulfate (IS)-treated cells. A) Enrichment plots showing the enrichment score (ES) with a large number of hits in IS-treated samples. B) Heatmaps showing the top 25 differentially expressed genes in the adipogenesis gene set, with upregulated (red) and downregulated (blue) proteins.

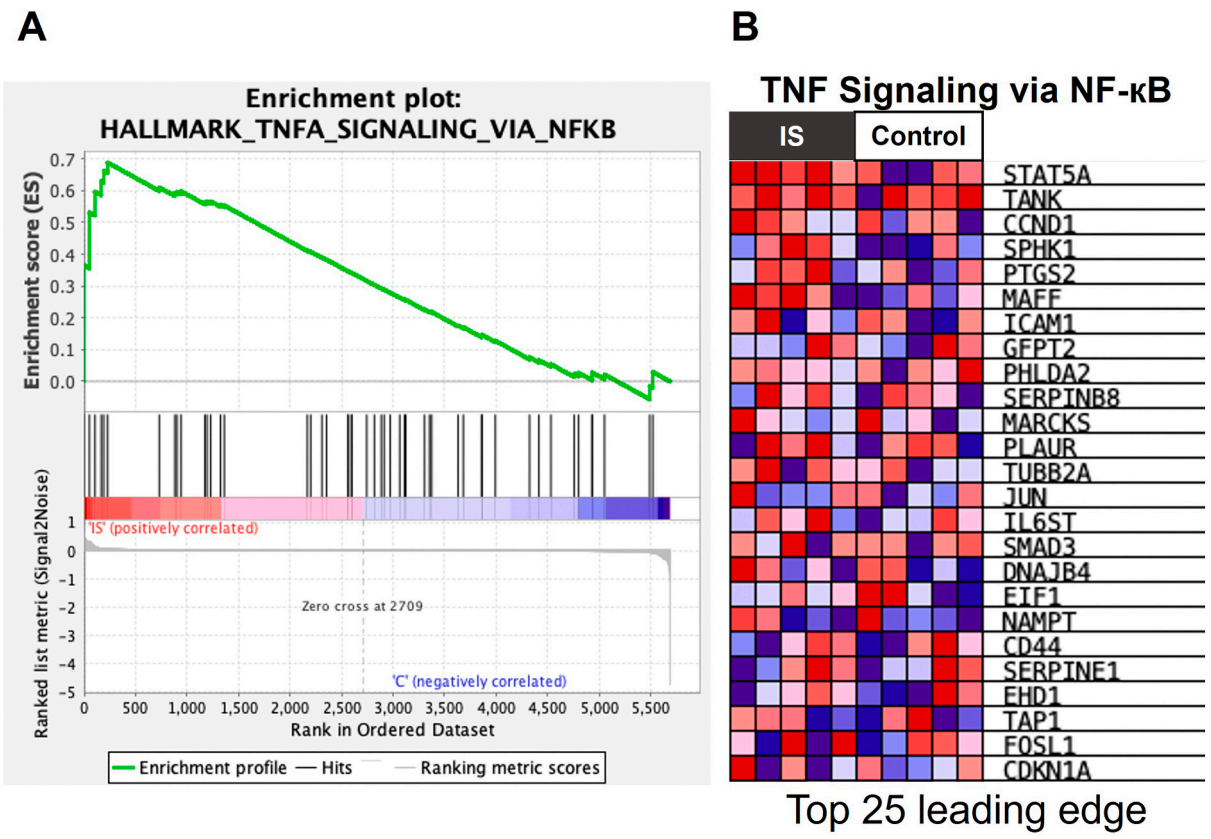

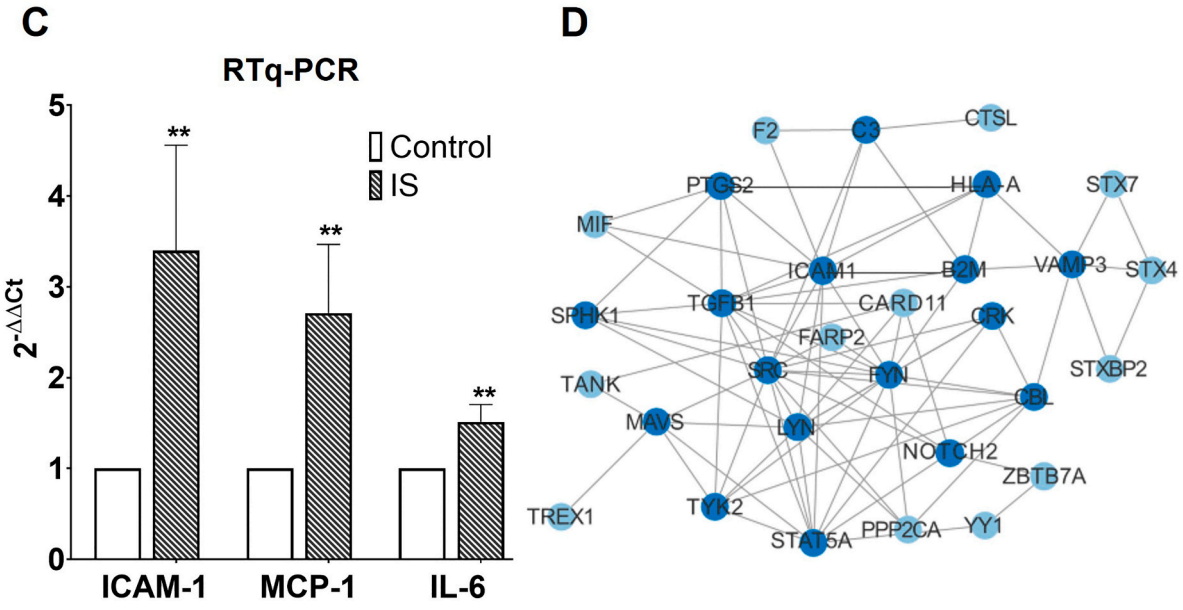

Fig. 4. GSEA revealed increased TNF signaling via NFκB in indoxyl sulfate (IS)-treated cells. A) Enrichment plots showing the enrichment score (ES) with a large number of hits in IS-treated samples. B) Heatmaps showing the top 25 differentially expressed genes in the "TNF signaling via NFκB" gene set, showing upregulated (red) and downregulated (blue) proteins. C) NFκB target genes were measured by RT-qPCR after IS treatment. mRNA expression is described as mean ± SD; a paired *t*-test was performed ** $p \leq 0.01$. D) Protein-protein interaction network formed by core enriched proteins from the analyzed inflammatory sets.

matrix (Fig. 7A, B), myogenesis (Fig. 7C, D), response to DNA damage caused by UV (Fig. 8A, B), and TNF signaling via NFκB (Fig. 9C, D). Enrichment plots and heatmaps of the principal proteins involved in these pathways are shown in Figs. 7 and 8. The core-enriched proteins are described in Table 2, and the interaction between these core proteins is represented by a network (Fig. 6D) that shows the alteration of different collagens, laminins, and fibrinogen. GSEA also suggests an association between the proteins upregulated in EV secreted by IS-treated endothelial cells and fatty acid metabolism. Although the nominal *p*-value was significant, the FDR *q*-value was too high, indicating

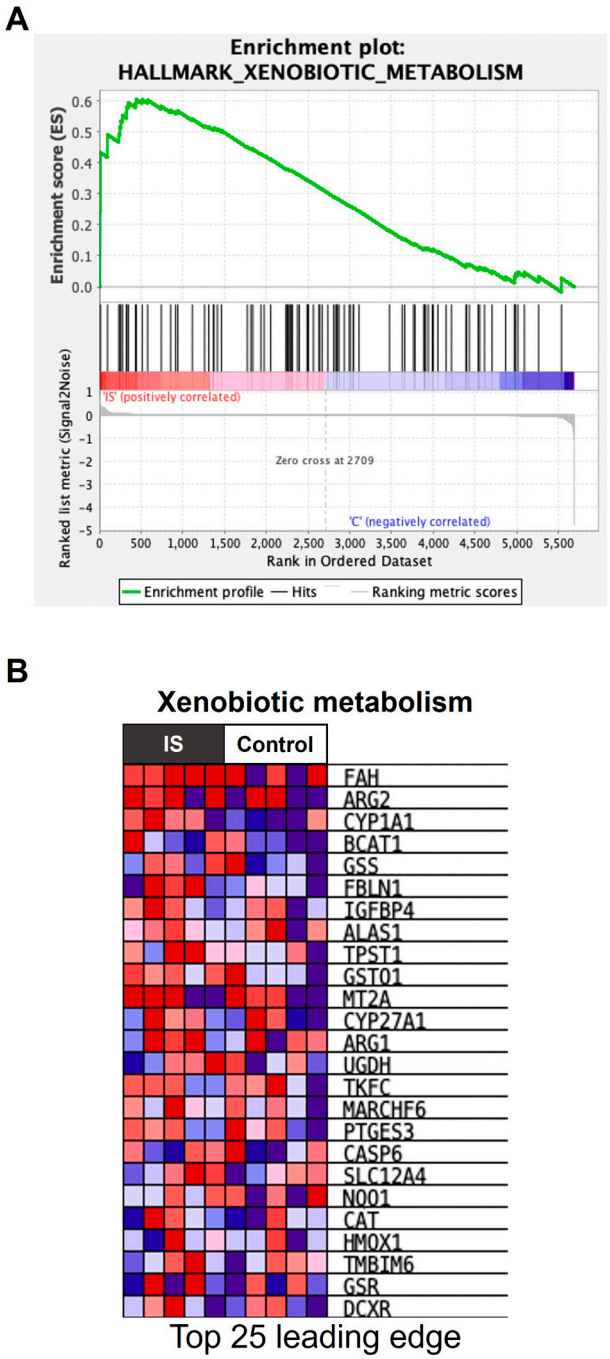

Fig. 5. GSEA revealed increased xenobiotic metabolism in indoxyl sulfate (IS)-treated cells. A) Enrichment plots showing the enrichment score (ES) with a large number of hits in IS-treated samples. B) Heatmaps showing the top 25 differentially expressed genes in the xenobiotic metabolism gene set, showing upregulated (red) and downregulated (blue) proteins.

insufficient certainty to confirm this hypothesis (Supplementary Fig. 3). Nevertheless, these results indicate a modification of the protein cargo of EVs, which could alter the functionality of their target cells or reflect the status of endothelial cells.

3.4. Concurrencies and discrepancies in protein expression in endothelial cells and their extracellular vesicles

Cells actively regulate the content of EVs, implying that changes in the cells translate into changes in the cargo of their EVs. Nevertheless, these changes are not always in the same direction; therefore, proteomic analysis of cells and EVs can provide complementary results. A Venn diagram was used to compare the up- and downregulated proteins found in endothelial cells and their EVs (Fig. 9A). In cells and their EVs, three proteins were upregulated (CYP1A1, MMP1, and RTN1) and three were downregulated (CTNNA2, H3C15, and H3-3A), whereas six proteins were downregulated in cells but upregulated in their EVs (ACTR1B, KRT16, KRT6A, KRT78, SERPINB3, and SFN). Proteins and their respective functions are listed in Table 3. MMP1 is a metalloprotease that participates in the degradation of the extracellular matrix, mainly collagen. Moreover, CYP1A1 is due to AhR activation by IS, the relevance of which is described in the Discussion section. Additionally, the proteins downregulated in cells and upregulated in EVs were primarily structural keratins, which points to a structural disorganization of the endothelium that may cause and increase vascular permeability.

4. Discussion

The mechanism by which uremic toxins induce endothelial dysfunction has not yet been completely elucidated. Further knowledge of this topic could help to identify potential therapeutic targets for detecting and preventing CVDs associated with CKD. In an in vitro model, the effect of the uremic toxin IS on the protein expression of endothelial cells and, more importantly, on the protein cargo of EVs was investigated. Proteomic analysis offers a large amount of information in a single experiment and offers deeper insights into endothelial damage in CKD. The integration of these types of analyses promises to help identify new potential biomarkers that could improve diagnostic tools and/or serve as novel therapeutic targets for kidney diseases [45].

Following the ISEV guidelines [29], EVs were characterized using different techniques. EVs express tetraspanins (CD9, CD63, and CD81), pan-EV markers that participate in EV biogenesis, and seem to be involved in EV cargo sorting and release [46,47]. Our sample comprised different types of EVs (exosomes and microvesicles based on their size), indicating that not all vesicles express these markers. Nevertheless, no differences were observed in EV characteristics after IS treatment compared with controls.

Our proteomic study of HUVECs revealed three pathways that were upregulated in response to IS treatment: adipogenesis, inflammation, and xenobiotic metabolism. IS treatment stimulated adipogenesis, which could be related to a pro-atherosclerotic effect that may be modulated by increased fatty acid production triggered by EVs. Atherosclerosis and atheroma plaque formation are the most common cardiovascular system disorders. In CKD, uremic toxin accumulation, aging endothelial cells, persistent inflammation, impaired lipid and electrolyte metabolism, and mitochondrial damage, among other factors, have been shown to increase the risk of atherosclerosis [9,48,49]. Uremic toxins are related to monocyte adhesion and migration through the endothelium, which favors atherosclerosis [17]. Uremic toxins may also affect perivascular adipose tissue, which participates in vascular function owing to its capacity to release anti-contractile and vasorelaxant factors. Under pathological conditions, such as obesity, adipose tissue is highly inflamed and increases the release of vasocontractile factors, some of which are associated with the renin-angiotensin-aldosterone system and pro-inflammatory factors, such as TNF [50,51]. Our results also showed an increase in inflammation and adipogenesis after treatment with IS, suggesting that this in vitro model could replicate the same conditions and mimic the mechanisms that participate in vascular dysfunction and the development of CVD in patients with CKD.

IS induces a pro-inflammatory status in the endothelium. Our proteomic analysis demonstrated the expression of several pro-inflammatory factors, including PTGS2 (COX-2), ICAM-1, complement (C3), and TGFB1, and proteins that act as mediators of the inflammatory signaling pathway, such as STAT5A, NOTCH2, FYN, and LYN. The upregulation of NFκB pathway end-products (ICAM-1, MCP-1, and IL-6)

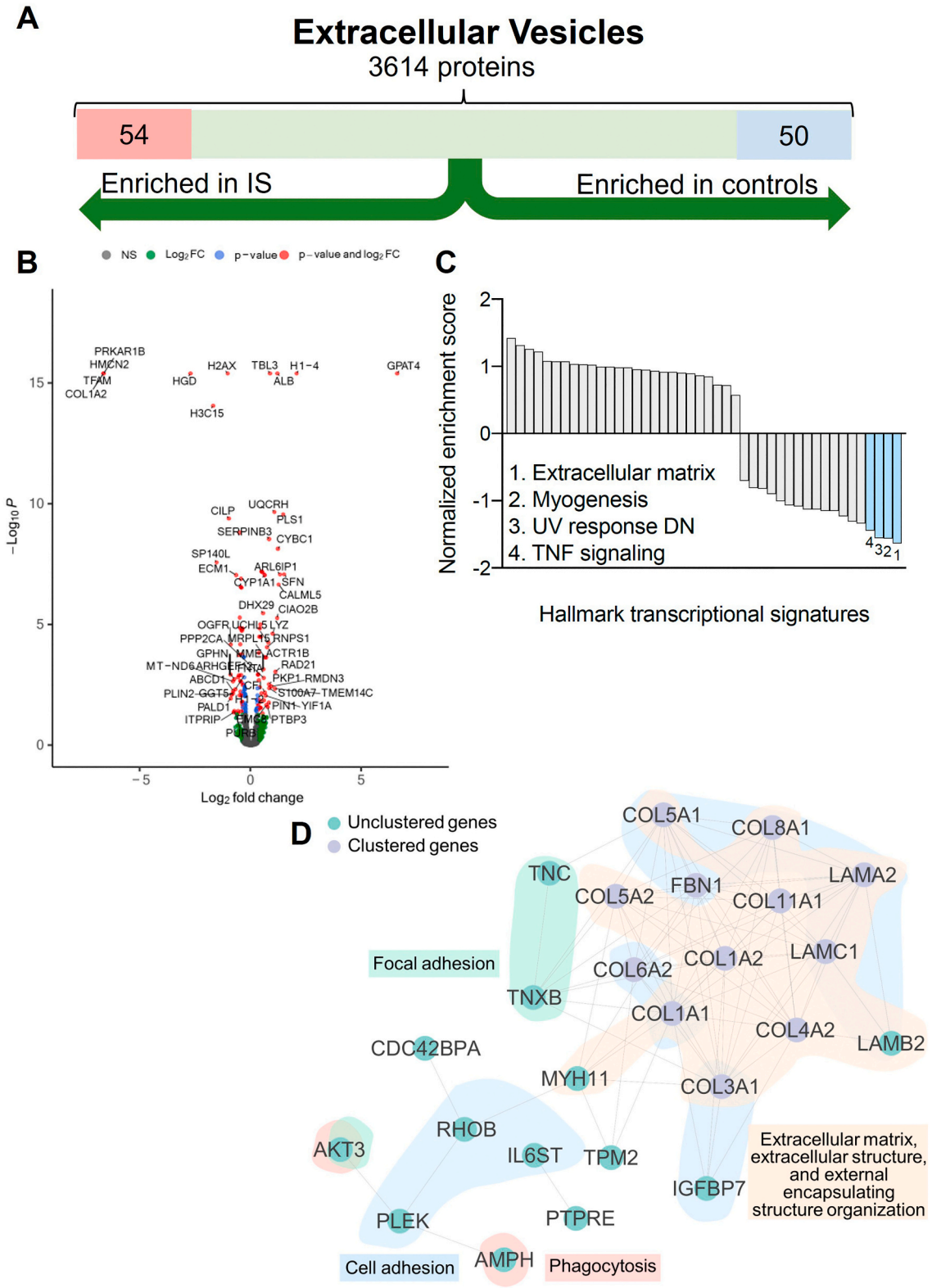

Fig. 6. Proteomic analysis of extracellular vesicles (EVs) from cells treated with indoxyl sulfate (IS) vs. controls (IS vs. C) ($n = 5$). A) A total of 3614 proteins with a q-value ≤ 0.01 (False Discovery Rate) were identified, of which 50 were more abundant in controls (blue) and 54 were more abundant in IS-treated EVs (red). B) Volcano plot displaying the proteins quantified according to their statistical significance and fold-change (FC). Differentially expressed proteins between the IS-treated and control groups with an adjusted p-value < 0.05 (FDR) and log2 of least 25 % are colored in red, with the proteins showing upregulation represented on the right (log2 FC > 0) and downregulation on the left (log2 FC < 0). Proteins with no significant differences (gray), a $\log_2$ FC (fold change) of at least 25 % (green), and an adjusted p-value < 0.05 (blue), are also shown. (C) GSEA revealed that four pathways were inhibited after IS treatment (blue). D) Protein-protein interaction network formed by the core enriched proteins of the suppressed pathways. The proteins participate in different functions represented by the border color: focal adhesion (green), cell adhesion (blue), phagocytosis (red), extracellular matrix, and external structure organization (light orange).

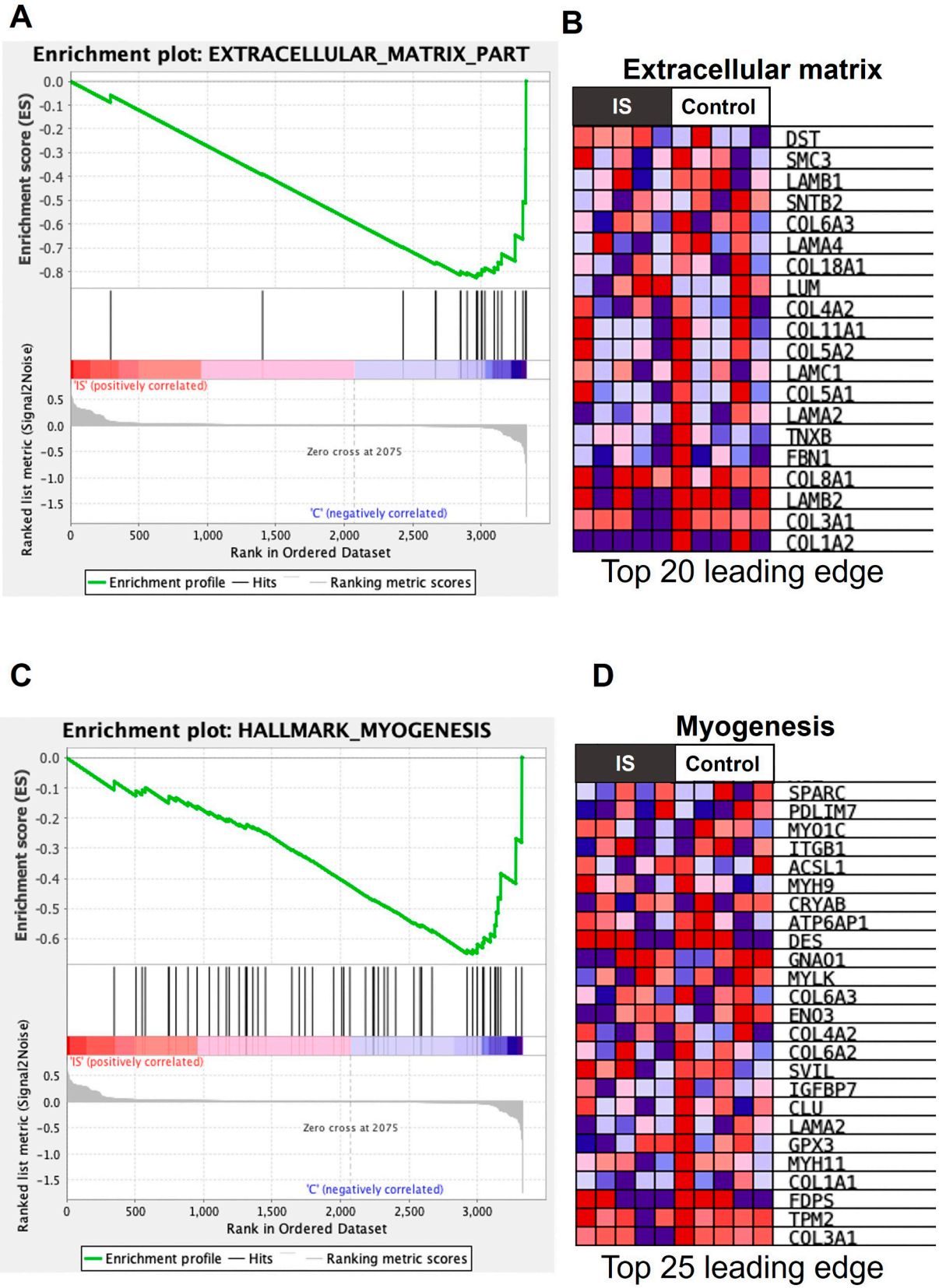

Fig. 7. GSEA revealed decreased extracellular matrix elements and myogenesis in extracellular vesicles (EVs) from indoxyl sulfate (IS)-treated cells. A) Enrichment plot and B) heatmap of extracellular matrix elements. C) Enrichment plot and D) heatmap of the myogenesis gene set. Enrichment plots show the enrichment score (ES) of our sample with a large number of hits in the controls. Heatmaps show the top 25 differentially expressed genes in the extracellular matrix elements and myogenesis gene sets, showing upregulated (red) and downregulated proteins (blue).

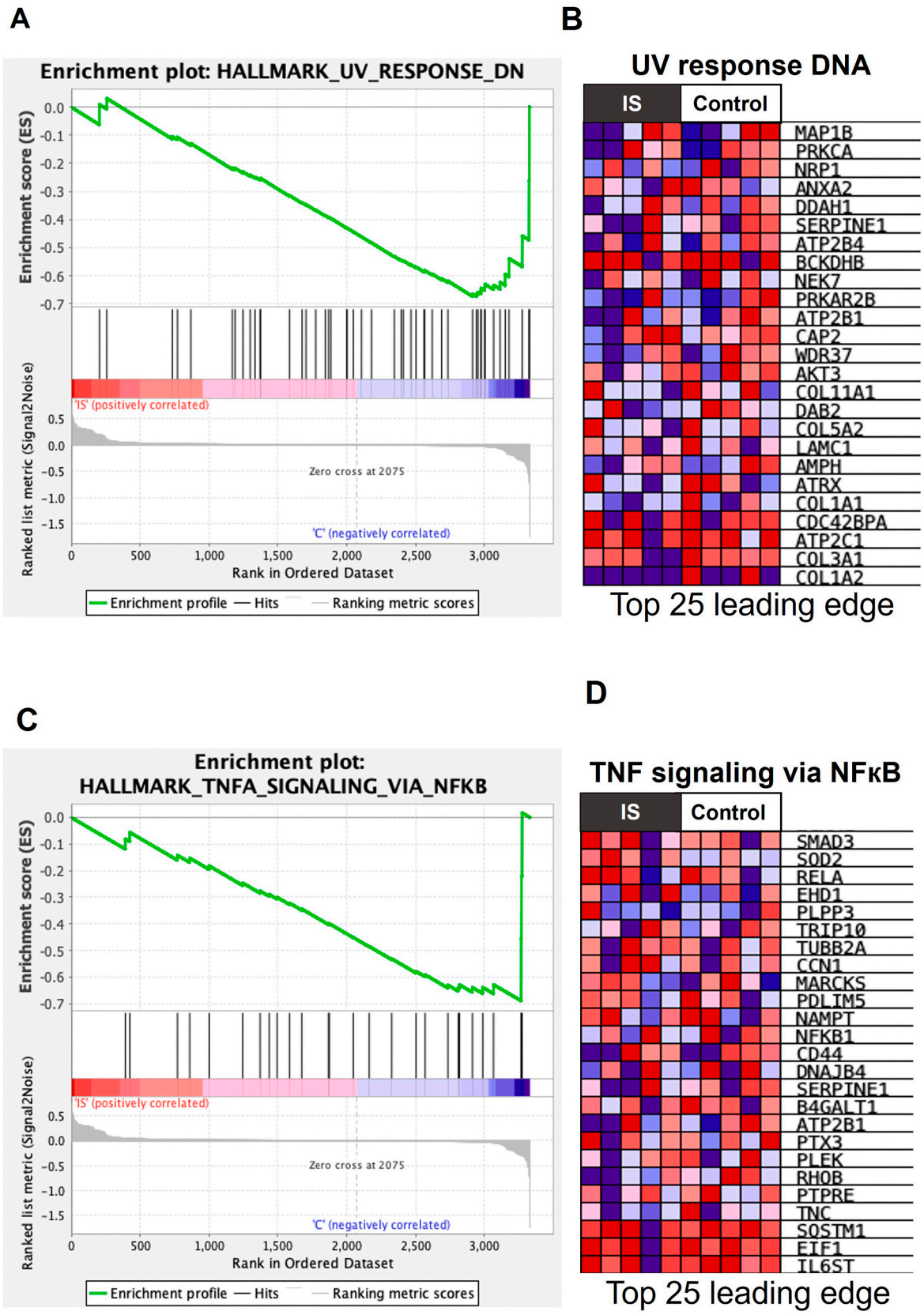

Fig. 8. GSEA analysis revealed downregulated proteins in response to UV and TNF signaling via NFκB in extracellular vesicles (EVs) from indoxyl sulfate (IS)-treated cells. A) Enrichment plot and B) heatmap of the genes downregulated in response to UV irradiation. C) Enrichment plot and D) heatmap of TNF signaling via NFκB. Enrichment plots show the enrichment score (ES) of our sample with a large number of hits in the controls. Heatmaps show the top 25 differentially expressed genes in the pathway gene set, showing upregulated proteins (red) and downregulated proteins (blue).

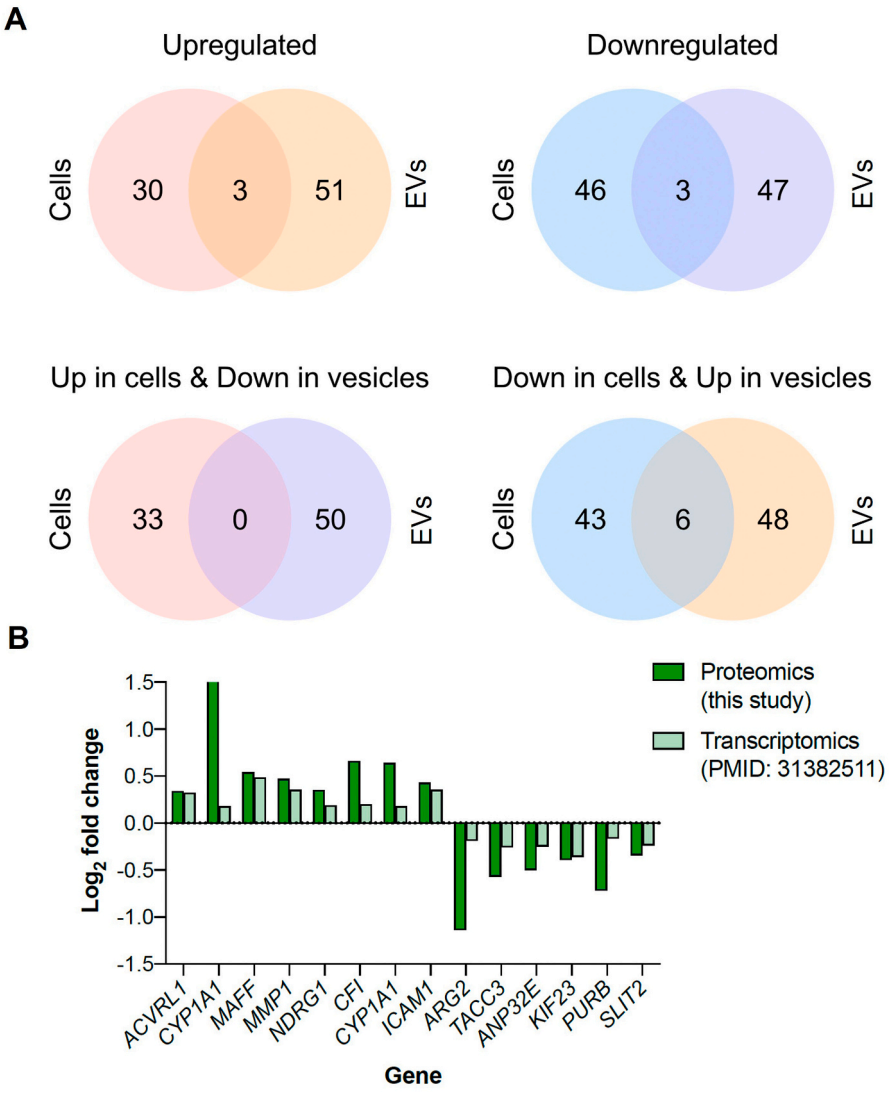

C

Protein	Up upon IS (cells)	Up upon IS (vesicles)	PMID31382511 *(Pei et al)* Up upon IS	*PMID34893640 (Diorio et al)* Up in disease	*PMID30499038 (Feldreich et al)* Up in disease
MMP1	Yes	Yes	Yes	Yes	Yes
CTSL	Yes	No	No	Yes	No

Fig. 9. Comparative study: A) Venn diagrams comparing differentially expressed proteins in cells and extracellular vesicles (EVs). B) Overlap of our study with a similar transcriptomic study found in the literature PMID31382511 [27] and C) overlap of our results with proteomic studies using plasma from different patients.

Table 1
Metabolic pathways were potentiated in endothelial cells after IS treatment.

Pathways	NES	NOM p-Value	FDR q-Value	Core enrichment
Adipogenesis	1.64	0.000	0.117	STAT5A, FAH, TANK, DNAJC15, COQ5, NDUFAB1, BCKDHA
TNF signaling via NFκB	1.58	0.006	0.117	STAT5A, TANK, CCND1, SPHK1, PTGS2, MAFF
Xenobiotic metabolism	1.53	0.012	0.140	FAH, ARG2, CYP1A1, BCAT1, GSS, FBLN1, IGFBP4, ALAS1, TPST1, GSTO1, MT2A, CYP27A1

revealed by RT-qPCR supported this hypothesis. COX-2 is an inducible pro-inflammatory enzyme involved in eicosanoid synthesis that may be relevant for treatment because it is the target of a large number of anti-inflammatory drugs. COX-2 activation is also relevant because, in response to UVB irradiation, AhR increases the expression of COX-2 mRNA [52], which is associated with other altered pathways. ICAM-1 is an adhesion molecule expressed on the surface of endothelial cells upon the activation of leukocyte extravasation. In addition, ICAM-1 is considered a marker of endothelial damage that favors CVDs [53]. MCP-1 has also been shown to exert adipogenic and angiogenic effects [54]. IL-6 is a predictive biomarker of atherosclerosis that contributes to plaque formation through metabolic, procoagulant, and endothelial

Table 2
Pathways downregulated in extracellular vesicles from endothelial cells after IS treatment.

Pathways	NES	NOM p-Value	FDR q-Value	Core enrichment
Extracellular matrix part	−1.63	0.003	0.003	COL4A2, COL11A1, COL5A2, LAMC1, COL5A1, LAMA2, TNXB, FBN1, COL8A1, LAMB2, COL3A1, COL1A2
Myogenesis	−1.56	0.009	0.220	ENO3, COL4A2, SVIL, IGFBP7, CLU, LAMA2, GPX3, MYH11, COL1A1, FDPS, TPM2, COL3A
Genes down-regulated in response to ultraviolet radiation	−1.56	0.014	0.111	CAP2, WDR37, AKT3, COL11A1, DAB2, COL5A2, LAMC1, AMPH, ATRX, COL1A1, CDC42BPA, ATP2C1, COL3A1, COL1A2
TNF signaling via NFκB	−1.56	0.041	0.202	PTX3, PLEK, RHOB, PTPRE, TNC, SQSTM1, EIF1, IL6ST

Table 3
Description of overlapping proteins in cells and extracellular vesicles.

Upregulated in cells and extracellular vesicles		
Protein	Gene	Description
Cytochrome P450 Family 1 Subfamily A Member 1	CYP1A1	Enzyme that inserts one oxygen atom into a substrate. Involved in the metabolism of various substrates (fatty acids, steroid hormones…)
Interstitial collagenase	MMP1	Involved in the breakdown of extracellular matrix, mainly collagens, in normal physiological processes.
Reticulon 1	RTN1	Associated with the endoplasmic reticulum, involved in neuroendocrine secretion or membrane trafficking in neuroendocrine cells.

Downregulated in cells and extracellular vesicles		
Protein	Gene	Description
Catenin α2	CTNNA2	Linker between cadherin adhesion receptors and the cytoskeleton to regulate cell-cell adhesion.
Histone 3 clustered 15	H3C15	Histones are proteins that links to DNA forming a nucleosome.
Histone 3 3A	H3-3A	Variant histone H3 which replaces conventional H3. It is predominant in non-dividing cells.

Downregulated in cells and upregulated in extracellular vesicles		
Protein	Gene	Description
Actin Related Protein 1B	ACTR1B	Component of a multi-subunit complex involved in microtubule-based vesicle motility. It is associated with the centrosome.
Keratin 16	KRT16	Cytokeratin type I. Acts as a structural constituent of the cytoskeleton.
Keratin 6A	KRT6A	Cytokeratin type II. Participates in wound healing and regulation of epithelial migration by inhibiting SRC.
Keratin 78	KRT78	Cytokeratin type II. Protein with intermediate filament domains.
Serpin B3	SERPINB3	Involved in several processes, including autocrine and paracrine signaling; and regulation of cellular protein metabolic process. Also functions as an apoptosis inhibitor via suppression of JNK1.
Stratifin	SFN	Cell cycle checkpoint protein that acts in response to DNA damage.

mechanisms [55], thereby contributing to CVD development. Chronic inflammation and oxidative stress contribute to cellular senescence and accelerate aging in CKD patients [56]. Furthermore, IL-6, ICAM-1, and MCP-1, as well as upregulation of MMP1 and alterations in collagen and fibronectin, have been associated with SASP [57], which may contribute to endothelial dysfunction and the development and propagation of CVDs associated with CKD. Moreover, to assess whether other proteins in this study were involved in SASP or senescence-related pathways, GSEA analysis was performed. In this case, GSEA analysis compared our ranked list of proteins from cells and extracellular vesicles with a recent study where the authors generated a senescence panel (named SenMayo) to characterize senescent cells at the single-cell level and identify key intercellular signaling pathways [58]. A comparison of our ranked list of proteins with the SenMayo list showed no significant results (Supplementary Fig. 4B), possibly because of the short treatment time with IS (24 h). A previous study by our group demonstrated that endothelial cells treated with IS for 72 h reached a senescent phenotype [22]. Nevertheless, the core enriched proteins of this analysis are shown in Supplementary Fig. 4A, in which ICAM-1 functions as a hub (interacts with multiple proteins).

Finally, IS is involved in xenobiotic metabolism because of its capacity to activate AhR, which binds to the xenobiotic response elements (XRE) present in DNA [59]. The binding of AhR to XRE reportedly promotes the expression of CYP1A1, CYP1A2, and CYP1B1 [60]. This is consistent with our proteomic results, wherein one of the most enriched proteins in IS-treated cells was CYP1A1. In addition, AhR participates in other biological functions such as vascular development, reproduction, and immune response (mediated by COX-2) [52]. Moreover, increased AhR expression and activation are associated with pathologies including preeclampsia, atherosclerosis, and hypertension, which are related to endothelial dysfunction [61]. In addition, animal studies have related AhR activation to gut microbiota modifications (which can increase IS production) and membranous nephropathy development [60]. It has also been reported that the activation of AhR by IS in red blood cells inhibits the activation of HIF, reducing the transcription of EPO, which causes anemia and predisposes patients to heart failure [62]. This is one of the potential mechanisms that may explain the commonly observed anemia in patients with CKD. The other is the capacity of IS to reduce proliferation and affect the viability of erythroid progenitors [63].

Proteomic analysis of EVs revealed four downregulated pathways: extracellular matrix elements, myogenesis, genes downregulated in response to UV, and TNF signaling via NFκB. EVs play an important role in the maintenance and repair of the extracellular matrix [64–66]. However, EVs released by damaged cells, such as those treated with IS, cannot perform these functions. A modification of extracellular matrix organization may be caused by the upregulation of metalloproteinases, such as MMP1, in cells and EVs. MMP1 is a factor in the SASP that is secreted to degrade the matrix and facilitate immune cell migration and

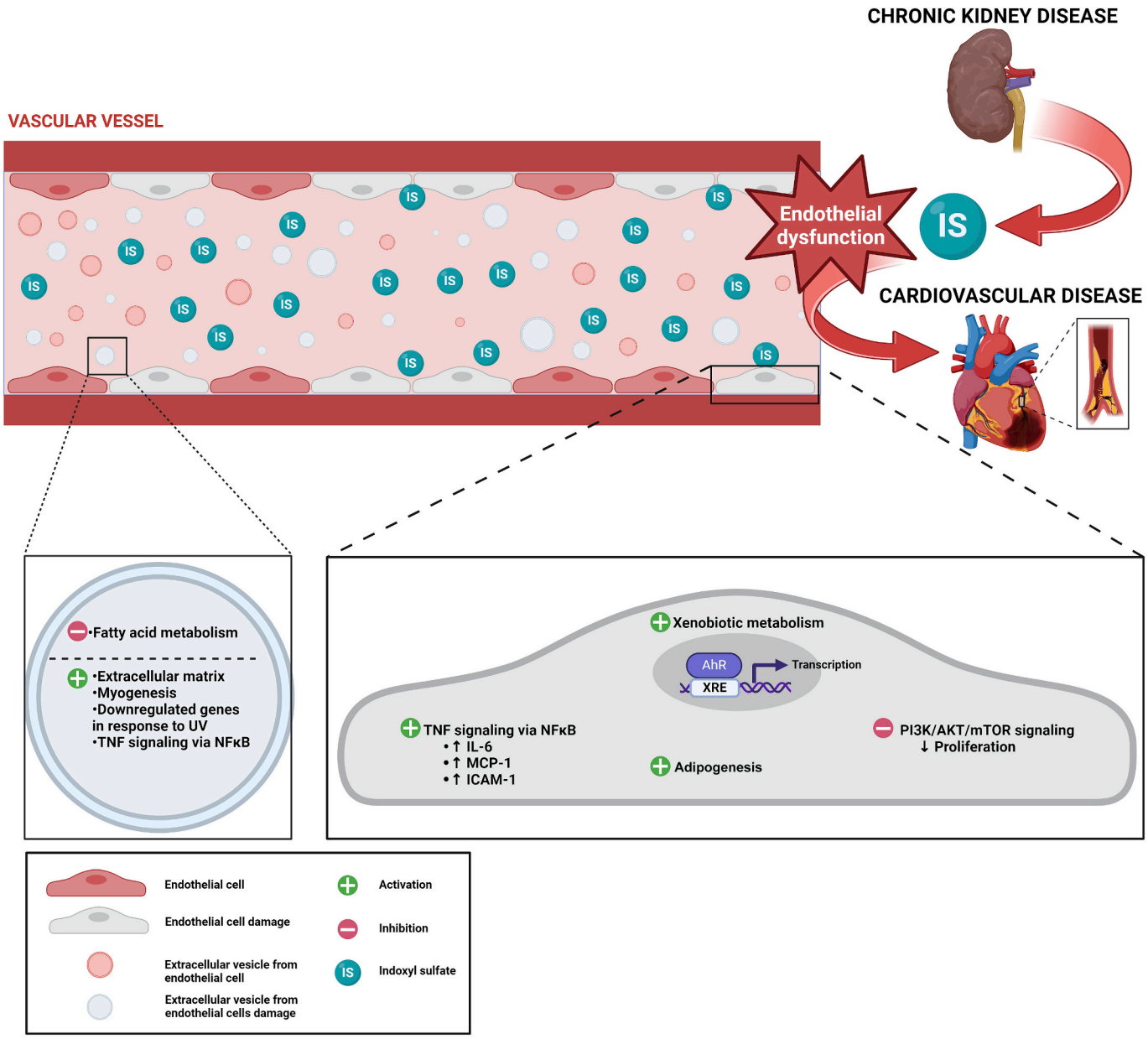

Fig. 10. Schematic representation of endothelial damage by indoxyl sulfate. In endothelial cells, indoxyl sulfate (IS) increased adipogenesis, inflammation, and xenobiotic metabolism and decreased proliferation via mTOR. Extracellular vesicles from indoxyl sulfate-treated cells present reduced levels of extracellular matrix elements, myogenesis-related factors, proteins downregulated by UV radiation, and fewer inflammatory factors. Together, these factors contribute to endothelial dysfunction characterized by chronic renal failure, and therefore, an increased risk of cardiovascular diseases in patients with chronic kidney disease.

extravasation. The SASP phenotype also includes alterations in extracellular matrix elements, such as collagen and laminin, as observed in our results. These findings support the idea that patients with CKD also exhibit the SASP phenotype due to premature aging. Our results also showed that the development of SASP originates from uremic toxins.

Factors related to myogenesis are also reduced in EVs from IS-treated cells, which could be linked to the sarcopenia commonly found in patients with CKD [67]. In addition, endothelial EVs are necessary for the correct functionality of vascular smooth muscle cells [68]; however, this functionality is also reduced owing to IS-induced damage.

A reduction in the expression of "genes downregulated in response to UV radiation," including cyclins and growth factors, was observed. This may indicate that damaged endothelial cells stopped releasing proliferative factors as a protective mechanism to avoid errors in cell replication. In other words, the cells tend to enter a senescent state to avoid or prevent cell damage.

Levels of proteins related to NF-κB signaling were reduced in EVs after IS treatment. This seems contradictory, considering that the same pathway is activated in cells. We propose that cells do not release inflammatory factors in EVs to avoid the dispersion of inflammation and reduce the risk of systemic inflammation. We investigated some factors related to the altered pathways using qPCR in cells treated with EVs; however, no differences were found. This may be due to the dose or treatment time, as the effect of EVs is dependent on dose, cell origin, and treatment time [69]. The modifications in EVs are relevant not only for the endothelium but also for other cell types. EV from IS-treated endothelial cells has been shown to induce vascular calcification [22], can induce endothelial progenitor cell dysfunction [70].

To validate our study, we compared our results with those reported in the literature. Pei et al. [27] performed RNA-seq on HUVECs treated with IS, and 14 concurrencies were found between the studies (Fig. 9B), helping validate our results. Proteomic profiling of the patient plasma

was also performed. Diorio et al. [71], who studied samples from children with multi-inflammatory syndromes, correlated their results with the development of hyperinflammation and vascular injury. In addition, Feldreich et al. [72] studied samples from patients with end-stage renal disease and found that proteins were associated with cardiovascular risk and vascular calcification. When comparing these studies with our results, MMP1 and CTSL (Fig. 9C) were consistently found to be associated with extracellular matrix degradation. These two proteins interfere with hyperinflammation, vascular injury, and CVD development, which are complications associated with CKD. Moreover, CTSL and MMP1 were overexpressed in the early stages of CKD development (as our study measured changes in protein expression only after 24 h of uremia). High plasma CSTL levels are associated with coronary artery disease [73] and increased CTSL activity correlates with proteinuria in patients with CKD [74], making this protein an attractive therapeutic target. In contrast, MMP1 is associated with myocardial infarction, senescence, and inflammation [75,76].

5. Conclusion

In this study, we investigated the mechanism by which EVs mediate endothelial dysfunction associated with renal damage caused by IS. Proteomic analysis of endothelial cells exposed to IS revealed increased adipogenesis, inflammation, and xenobiotic metabolism, and decreased proliferation via mTOR. Inflammation through NF-κB was confirmed by elevated levels of end products (IL-6, MCP-1, and ICAM-1). EVs from IS-treated cells exhibited reduced extracellular matrix elements, myogenesis-related factors, proteins downregulated by UV radiation, and fewer inflammatory factors. These endothelial alterations align with SASP, suggesting that IS contributes to premature aging in CKD (Fig. 10).

Therefore, this study provides a new perspective on the cellular pathways underlying IS-induced endothelial dysfunction, emphasizing the roles of inflammation and atherosclerosis development. Understanding these mechanisms may offer new possibilities for targeting CKD-related issues. These findings hold the potential for the development of diagnostic and therapeutic tools for CVDs associated with CKD, even in the early stages.

Supplementary data to this article can be found online at https://doi.org/10.1016/j.lfs.2024.122810.

CRediT authorship contribution statement

Andrea Figuer: Writing – original draft, Validation, Methodology, Formal analysis, Data curation. **Fátima M. Santos:** Writing – review & editing, Validation, Supervision, Software, Methodology, Investigation, Formal analysis, Data curation. **Sergio Ciordia:** Writing – review & editing, Validation, Software, Formal analysis, Data curation. **Gemma Valera:** Writing – review & editing, Investigation, Formal analysis, Data curation. **Beatriz Martín-Jouve:** Writing – review & editing, Validation, Methodology, Formal analysis, Data curation. **Juan Pablo Hernández-Fonseca:** Writing – review & editing, Validation, Methodology, Formal analysis, Data curation. **Guillermo Bodega:** Writing – review & editing, Writing – original draft, Visualization, Validation, Supervision, Methodology, Investigation. **Noemí Ceprián:** Writing – review & editing, Validation, Methodology, Investigation, Formal analysis. **Rafael Ramírez:** Writing – review & editing, Visualization, Supervision, Resources, Project administration. **Julia Carracedo:** Writing – review & editing, Validation, Supervision, Resources, Funding acquisition, Conceptualization. **Matilde Alique:** Writing – review & editing, Writing – original draft, Validation, Supervision, Resources, Project administration, Methodology, Investigation, Funding acquisition, Conceptualization.

Declaration of competing interest

The authors declare that they have no conflicts of interest related to the content of this article.

Acknowledgments

Extracellular vesicle characterization and analysis were carried out at the Extracellular Vesicles Unit (UVEx) of the Hospital Nacional Parapléjicos (SESCAM). In addition, we acknowledge the EGO Genomics, particularly Dr. Luis F. Lorenzo and Dr. Laura Clavaín for their assistance with the bioinformatics analysis. In addition, we thank IESMAT for providing the nanoparticle tracking analysis results.

Funding

This research was funded by grants from the Instituto de Salud Carlos III (ISCIII) and cofounded by Fondo Europeo de Desarrollo Regional (FEDER): "PI19/00240", "PI20/01321", and "PI23/01109". A.F. enjoyed the PFIS contract "FI20/00018" and F.M.S. a Sara Borrel "CD23/00049." Also, G.V. received a contract from the Instituto de Investigación Sanitario del Hospital Universitario 12 de Octubre (i + 12) "I + 12-AY2OO414-1". In addition, grants from Universidad de Alcalá ("Ayuda de la Línea de Actuación Excelencia para el Profesorado Universitario de la UAH"; EPU-INV-UAH/2022/001), RICORS2040; RD21/0005/0002 funded by European Union—NextGenerationEU and Comunidad de Madrid (CAM; P2022/BMD-7223 CIFRA_COR-CM), supported this work.

References

[1] A.S. Levey, R. Atkins, J. Coresh, E.P. Cohen, A.J. Collins, K.-U. Eckardt, M.E. Nahas, B.L. Jaber, M. Jadoul, A. Levin, N.R. Powe, J. Rossert, D.C. Wheeler, N. Lameire, G. Eknoyan, Chronic kidney disease as a global public health problem: approaches and initiatives – a position statement from Kidney Disease Improving Global Outcomes, Kidney Int. 72 (2007) 247–259, https://doi.org/10.1038/sj.ki.5002343.

[2] C.P. Kovesdy, Epidemiology of chronic kidney disease: an update 2022, Kidney Int. Suppl. 12 (2022) (2011) 7–11, https://doi.org/10.1016/J.KISU.2021.11.003.

[3] C. Chen, S. Ding, J. Wang, Digital health for aging populations, Nat. Med. 29 (2023) 1623–1630, https://doi.org/10.1038/s41591-023-02391-8.

[4] A. Figuer, M. Alique, G. Valera, N. Serroukh, N. Ceprían, P. de Sequera, E. Morales, J. Carracedo, R. Ramírez, G. Bodega, New mechanisms involved in the development of cardiovascular disease in chronic kidney disease, Nefrología (English Edition) 43 (2023) 63–80, https://doi.org/10.1016/j.nefroe.2023.05.014.

[5] C. Vida, C. Oliva, C. Yuste, N. Ceprián, P.J. Caro, G. Valera, I. González de Pablos, E. Morales, J. Carracedo, Oxidative stress in patients with advanced CKD and renal replacement therapy: the key role of peripheral blood leukocytes, Antioxidants 10 (2021) 1155, https://doi.org/10.3390/antiox10071155.

[6] A. Merino, S. Nogueras, P. Buendía, R. Ojeda, J. Carracedo, R. Ramirez-Chamond, A. Martin-Malo, P. Aljama, Microinflammation and endothelial damage in hemodialysis, Hemodialysis-From Basic Research to Clinical Trials (2008) 83–88, https://doi.org/10.1159/000130412.

[7] W.E. White, Aging and uremia: is there cellular and molecular crossover? World J Nephrol 4 (2015) 19, https://doi.org/10.5527/wjn.v4.i1.19.

[8] A. Ugusman, J. Kumar, A. Aminuddin, Endothelial function and dysfunction: impact of sodium-glucose cotransporter 2 inhibitors, Pharmacol. Ther. 224 (2021) 107832, https://doi.org/10.1016/j.pharmthera.2021.107832.

[9] R. Ramírez, N. Ceprian, A. Figuer, G. Valera, G. Bodega, M. Alique, J. Carracedo, Endothelial senescence and the chronic vascular diseases: challenges and therapeutic opportunities in atherosclerosis, J Pers Med 12 (2022) 215, https://doi.org/10.3390/jpm12020215.

[10] J. Carracedo, M. Alique, C. Vida, G. Bodega, N. Ceprián, E. Morales, M. Praga, P. de Sequera, R. Ramírez, Mechanisms of cardiovascular disorders in patients with chronic kidney disease: a process related to accelerated senescence, Front. Cell Dev. Biol. 8 (2020), https://doi.org/10.3389/fcell.2020.00185.

[11] C. Mas-Bargues, M. Alique, M.T. Barrús-Ortiz, C. Borrás, R. Rodrigues-Díez, Exploring new kingdoms: the role of extracellular vesicles in oxi-inflamm-aging related to cardiorenal syndrome, Antioxidants 11 (2021) 78, https://doi.org/10.3390/antiox11010078.

[12] A. Figuer, G. Bodega, P. Tato, G. Valera, N. Serroukh, N. Ceprian, P. de Sequera, E. Morales, J. Carracedo, R. Ramírez, M. Alique, Premature aging in chronic kidney disease: the outcome of persistent inflammation beyond the bounds, Int. J. Environ. Res. Public Health 18 (2021) 8044, https://doi.org/10.3390/ijerph18158044.

[13] W.-J. Wang, G.-Y. Cai, X.-M. Chen, Cellular senescence, senescence-associated secretory phenotype, and chronic kidney disease, Oncotarget 8 (2017) 64520–64533, https://doi.org/10.18632/oncotarget.17327.

[14] M. Alique, R. Ramírez-Carracedo, G. Bodega, J. Carracedo, R. Ramírez, Senescent microvesicles: a novel advance in molecular mechanisms of atherosclerotic

calcification, Int. J. Mol. Sci. 19 (2018) 2003, https://doi.org/10.3390/ijms19072003.
[15] I. Filipska, A. Winiarska, M. Knysak, T. Stompór, Contribution of gut microbiota-derived uremic toxins to the cardiovascular system mineralization, Toxins (Basel) 13 (2021) 274, https://doi.org/10.3390/toxins13040274.
[16] F. Guerrero, A. Carmona, M.J. Jimenez, T. Obrero, V. Pulido, J.A. Moreno, S. Soriano, A. Martín-Malo, P. Aljama, Passage number-induced replicative senescence modulates the endothelial cell response to protein-bound uremic toxins, Toxins (Basel) 13 (2021) 738, https://doi.org/10.3390/toxins13100738.
[17] A. Carmona, F. Guerrero, J.R. Muñoz-Castañeda, M.J. Jimenez, M. Rodriguez, S. Soriano, A. Martin-Malo, Uremic toxins induce THP-1 monocyte endothelial adhesion and migration through specific mi RNA expression, Int. J. Mol. Sci. 24 (2023) 12938, https://doi.org/10.3390/ijms241612938.
[18] Y.J. Lim, N.A. Sidor, N.C. Tonial, A. Che, B.L. Urquhart, Uremic toxins in the progression of chronic kidney disease and cardiovascular disease: mechanisms and therapeutic targets, Toxins (Basel) 13 (2021) 142, https://doi.org/10.3390/toxins13020142.
[19] F. Meziani, A. Tesse, R. Andriantsitohaina, Microparticles are vectors of paradoxical information in vascular cells including the endothelium: role in health and diseases, Pharmacol. Rep. 60 (2008) 75–84.
[20] T. Asao, G.C. Tobias, S. Lucotti, D.R. Jones, I. Matei, D. Lyden, Extracellular vesicles and particles as mediators of long-range communication in cancer: connecting biological function to clinical applications, Extracellular Vesicles and Particles as Mediators of Long-Range Communication in Cancer: Connecting Biological Function to Clinical Applications 4 (2023) 461–485, https://doi.org/10.20517/evcna.2023.37.
[21] A. Carmona, M.L. Agüera, C. Luna-Ruiz, P. Buendía, L. Calleros, A. García-Jerez, M. Rodríguez-Puyol, M. Arias, M. Arias-Guillen, G. de Arriba, J. Ballarin, C. Bernis, E. Fernández, S. García-Rebollo, J. Mancha, G. del Peso, E. Pérez, E. Poch, J. M. Portolés, D. Rodríguez-Puyol, R. Sánchez-Villanueva, F. Sarro, A. Torres, A. Martín-Malo, P. Aljama, R. Ramírez, J. Carracedo, Markers of endothelial damage in patients with chronic kidney disease on hemodialysis, American Journal of Physiology-Renal Physiology 312 (2017) F673–F681, https://doi.org/10.1152/ajprenal.00013.2016.
[22] M. Alique, G. Bodega, E. Corchete, E. García-Menéndez, P. de Sequera, R. Luque, D. Rodríguez-Padrón, M. Marqués, J. Portolés, J. Carracedo, R. Ramírez, Microvesicles from indoxyl sulfate-treated endothelial cells induce vascular calcification in vitro, Comput. Struct. Biotechnol. J. 18 (2020) 953–966, https://doi.org/10.1016/j.csbj.2020.04.006.
[23] H. Alqurashi, M. Alsharief, M.L. Perciato, B. Raven, K. Ren, D.W. Lambert, Message in a bubble: the translational potential of extracellular vesicles, J. Physiol. 601 (2023) 4895–4905, https://doi.org/10.1113/JP282047.
[24] A. Schubert, M. Boutros, Extracellular vesicles and oncogenic signaling, Mol. Oncol. 15 (2021) 3–26, https://doi.org/10.1002/1878-0261.12855.
[25] Z. Lu, F. Lu, Y. Zheng, Y. Zeng, C. Zou, X. Liu, Grape seed proanthocyanidin extract protects human umbilical vein endothelial cells from indoxyl sulfate-induced injury via ameliorating mitochondrial dysfunction, Ren. Fail. 38 (2016) 100–108, https://doi.org/10.3109/0886022X.2015.1104609.
[26] C.-J. Lin, H.-H. Chen, C.-F. Pan, C.-K. Chuang, T.-J. Wang, F.-J. Sun, C.-J. Wu, p-Cresylsulfate and indoxyl sulfate level at different stages of chronic kidney disease, J. Clin. Lab. Anal. 25 (2011) 191–197, https://doi.org/10.1002/jcla.20456.
[27] J. Pei, R. Juni, M. Harakalova, D.J. Duncker, F.W. Asselbergs, P. Koolwijk, V. van Hinsbergh, M.C. Verhaar, M. Mokry, C. Cheng, Indoxyl sulfate stimulates angiogenesis by regulating reactive oxygen species production via CYP1B1, Toxins (Basel) 11 (2019) 454, https://doi.org/10.3390/toxins11080454.
[28] X. Li, Z. Lu, F. Zhou, W. Jin, Y. Yang, S. Chen, Z. Xie, Y. Zhao, Indoxyl sulfate promotes the atherosclerosis through up-regulating the miR-34a expression in endothelial cells and vascular smooth muscle cells in vitro, Vascul. Pharmacol. 131 (2020) 106763, https://doi.org/10.1016/j.vph.2020.106763.
[29] J.A. Welsh, D.C.I. Goberdhan, L. O'Driscoll, E.I. Buzas, C. Blenkiron, B. Bussolati, H. Cai, D. Di Vizio, T.A.P. Driedonks, U. Erdbrügger, J.M. Falcon-Perez, Q. Fu, A. F. Hill, M. Lenassi, S.K. Lim, M.G. Mahoney, S. Mohanty, A. Möller, R. Nieuwland, T. Ochiya, S. Sahoo, A.C. Torrecilhas, L. Zheng, A. Zijlstra, S. Abuelreich, R. Bagabas, P. Bergese, E.M. Bridges, M. Brucale, D. Burger, R.P. Carney, E. Cocucci, F. Colombo, R. Crescitelli, E. Hanser, A.L. Harris, N.J. Haughey, A. Hendrix, A.R. Ivanov, T. Jovanovic-Talisman, N.A. Kruh-Garcia, V. Ku'ulei-Lyn Faustino, D. Kyburz, C. Lässer, K.M. Lennon, J. Lötvall, A.L. Maddox, E.S. Martens-Uzunova, R.R. Mizenko, L.A. Newman, A. Ridolfi, E. Rohde, T. Rojalin, A. Rowland, A. Saftics, U.S. Sandau, J.A. Saugstad, F. Shekari, S. Swift, D. Ter-Ovanesyan, J.P. Tosar, Z. Useckaite, F. Valle, Z. Varga, E. van der Pol, M.J.C. van Herwijnen, M.H.M. Wauben, A.M. Wehman, S. Williams, A. Zendrini, A. J. Zimmerman, MISEV Consortium, C. Théry, K.W. Witwer, Minimal information for studies of extracellular vesicles (MISEV2023): from basic to advanced approaches, J Extracell Vesicles 13 (2024), https://doi.org/10.1002/jev2.12404.
[30] J.A. Welsh, E. Van Der Pol, G.J.A. Arkesteijn, M. Bremer, A. Brisson, F. Coumans, F. Dignat-George, E. Duggan, I. Ghiran, B. Giebel, A. Görgens, A. Hendrix, R. Lacroix, J. Lannigan, S.F.W.M. Libregts, E. Lozano-Andrés, A. Morales-Kastresana, S. Robert, L. De Rond, T. Tertel, J. Tigges, O. De Wever, X. Yan, R. Nieuwland, M.H.M. Wauben, J.P. Nolan, J.C. Jones, MIFlowCyt-EV: a framework for standardized reporting of extracellular vesicle flow cytometry experiments, J Extracell Vesicles 9 (2020), https://doi.org/10.1080/20013078.2020.1713526.
[31] S. Ciordia, G. Alvarez-Sola, M. Rullán, J.M. Urman, M.A. Ávila, F.J. Corrales, Digging deeper into bile proteome, J. Proteomics 230 (2021) 103984, https://doi.org/10.1016/j.jprot.2020.103984.
[32] S. Ciordia, G. Alvarez-Sola, M. Rullán, J.M. Urman, M.A. Ávila, F.J. Corrales, Bile processing protocol for improved proteomic analysis, Methods Mol. Biol. (2022) 1–10, https://doi.org/10.1007/978-1-0716-1936-0_1.
[33] S.M. Rocha, F.M. Santos, S. Socorro, L.A. Passarinha, C.J. Maia, Proteomic analysis of STEAP1 knockdown in human LNCaP prostate cancer cells, Biochimica et Biophysica Acta (BBA) - Molecular Cell Research 2023 (1870) 119522, https://doi.org/10.1016/j.bbamcr.2023.119522.
[34] L. Guerrero, L. Carmona-Rodríguez, F.M. Santos, S. Ciordia, L. Stark, L. Hierro, P. Pérez-Montero, D. Vicent, F.J. Corrales, Molecular basis of progressive familial intrahepatic cholestasis 3. A proteomics study, BioFactors (2024), https://doi.org/10.1002/biof.2041.
[35] et al. Olmo, E.M., Ciordia, S, Santos, FM, Proteomic snapshot of saliva samples predicts new pathways implicated in SARS-CoV-2 pathogenesis. Clin. Proteomics, (n.d.). doi:https://doi.org/10.1186/s12014-024-09482-9.
[36] Y. Perez-Riverol, J. Bai, C. Bandla, D. García-Seisdedos, S. Hewapathirana, S. Kamatchinathan, D.J. Kundu, A. Prakash, A. Frericks-Zipper, M. Eisenacher, M. Walzer, S. Wang, A. Brazma, J.A. Vizcaíno, The PRIDE database resources in 2022: a hub for mass spectrometry-based proteomics evidences, Nucleic Acids Res. 50 (2022) D543–D552, https://doi.org/10.1093/nar/gkab1038.
[37] L.M. Blighe K, S. Rana, EnhancedVolcano: Publication-Ready Volcano Plots With Enhanced Colouring and Labeling, 2023, https://doi.org/10.18129/B9.bioc.EnhancedVolcano.
[38] A. Subramanian, P. Tamayo, V.K. Mootha, S. Mukherjee, B.L. Ebert, M.A. Gillette, A. Paulovich, S.L. Pomeroy, T.R. Golub, E.S. Lander, J.P. Mesirov, Gene set enrichment analysis: a knowledge-based approach for interpreting genome-wide expression profiles, Proc. Natl. Acad. Sci. 102 (2005) 15545–15550, https://doi.org/10.1073/pnas.0506580102.
[39] A. Liberzon, C. Birger, H. Thorvaldsdóttir, M. Ghandi, J.P. Mesirov, P. Tamayo, The molecular signatures database hallmark gene set collection, Cell Syst. 1 (2015) 417–425, https://doi.org/10.1016/j.cels.2015.12.004.
[40] D. Szklarczyk, A. Franceschini, S. Wyder, K. Forslund, D. Heller, J. Huerta-Cepas, M. Simonovic, A. Roth, A. Santos, K.P. Tsafou, M. Kuhn, P. Bork, L.J. Jensen, C. von Mering, STRING v10: protein–protein interaction networks, integrated over the tree of life, Nucleic Acids Res. 43 (2015) D447–D452, https://doi.org/10.1093/nar/gku1003.
[41] P. Shannon, A. Markiel, O. Ozier, N.S. Baliga, J.T. Wang, D. Ramage, N. Amin, B. Schwikowski, T. Ideker, Cytoscape: a software environment for integrated models of biomolecular interaction networks, Genome Res. 13 (2003) 2498–2504, https://doi.org/10.1101/gr.1239303.
[42] N. Balestrieri, V. Palzkill, C. Pass, J. Tan, Z.R. Salyers, C. Moparthy, A. Murillo, K. Kim, T. Thome, Q. Yang, K.A. O'Malley, S.A. Berceli, F. Yue, S.T. Scali, L. F. Ferreira, T.E. Ryan, Activation of the aryl hydrocarbon receptor in muscle exacerbates ischemic pathology in chronic kidney disease, Circ. Res. 133 (2023) 158–176, https://doi.org/10.1161/CIRCRESAHA.123.322875.
[43] J.S.L. Yu, W. Cui, Proliferation, survival and metabolism: the role of PI3K/AKT/mTOR signalling in pluripotency and cell fate determination, Development 143 (2016) 3050–3060, https://doi.org/10.1242/dev.137075.
[44] C. López-Otín, M.A. Blasco, L. Partridge, M. Serrano, G. Kroemer, The hallmarks of aging, Cell 153 (2013) 1194–1217, https://doi.org/10.1016/j.cell.2013.05.039.
[45] P. Schlosser, M.E. Grams, E.P. Rhee, Proteomics: progress and promise of high-throughput proteomics in chronic kidney disease, Mol. Cell. Proteomics 22 (2023) 100550, https://doi.org/10.1016/j.mcpro.2023.100550.
[46] A. Giovanazzi, M.J.C. van Herwijnen, M. Kleinjan, G.N. van der Meulen, M.H. M. Wauben, Surface protein profiling of milk and serum extracellular vesicles unveils body fluid-specific signatures, Sci. Rep. 13 (2023) 8758, https://doi.org/10.1038/s41598-023-35799-w.
[47] J. Jankovičová, P. Sečová, K. Michalková, J. Antalíková, Tetraspanins, more than markers of extracellular vesicles in reproduction, Int. J. Mol. Sci. 21 (2020) 7568, https://doi.org/10.3390/ijms21207568.
[48] P. Fularski, J. Krzemińska, N. Lewandowska, E. Młynarska, M. Saar, M. Wronka, J. Rysz, B. Franczyk, Statins in chronic kidney disease—effects on atherosclerosis and cellular senescence, Cells 12 (2023) 1679, https://doi.org/10.3390/cells12131679.
[49] H. Nishizawa, N. Maeda, I. Shimomura, Impact of hyperuricemia on chronic kidney disease and atherosclerotic cardiovascular disease, Hypertens. Res. 45 (2022) 635–640, https://doi.org/10.1038/s41440-021-00840-w.
[50] P. Gu, A. Xu, Interplay between adipose tissue and blood vessels in obesity and vascular dysfunction, Rev. Endocr. Metab. Disord. 14 (2013) 49–58, https://doi.org/10.1007/s11154-012-9230-8.
[51] T. Szasz, G.F. Bomfim, R.C. Webb, The influence of perivascular adipose tissue on vascular homeostasis, Vasc Health Risk Manag (2013) 105, https://doi.org/10.2147/VHRM.S33760.
[52] E. Fritsche, C. Schäfer, C. Calles, T. Bernsmann, T. Bernshausen, M. Wurm, U. Hübenthal, J.E. Cline, H. Hajimiragha, P. Schroeder, L.-O. Klotz, A. Rannug, P. Fürst, H. Hanenberg, J. Abel, J. Krutmann, Lightening up the UV response by identification of the arylhydrocarbon receptor as a cytoplasmatic target for ultraviolet B radiation, Proc. Natl. Acad. Sci. 104 (2007) 8851–8856, https://doi.org/10.1073/pnas.0701764104.
[53] V. Singh, R. Kaur, P. Kumari, C. Pasricha, R. Singh, ICAM-1 and VCAM-1: gatekeepers in various inflammatory and cardiovascular disorders, Clin. Chim. Acta 548 (2023) 117487, https://doi.org/10.1016/j.cca.2023.117487.
[54] Z. Zhu, L. Guo, N. Yeltai, H. Xu, Y. Zhang, Chemokine (C-C motif) ligand 2-enhanced adipogenesis and angiogenesis of human adipose-derived stem cell and human umbilical vein endothelial cell co-culture system in adipose tissue engineering, J. Tissue Eng. Regen. Med. 16 (2022) 163–176, https://doi.org/10.1002/term.3264.

[55] B. Friedrich, D. Alexander, A. Janessa, H.-U. Häring, F. Lang, T. Risler, Acute effects of hemodialysis on cytokine transcription profiles: evidence for C-reactive protein-dependency of mediator induction, Kidney Int. 70 (2006) 2124–2130, https://doi.org/10.1038/sj.ki.5001865.
[56] T. Ebert, S.-C. Pawelzik, A. Witasp, S. Arefin, S. Hobson, K. Kublickiene, P.G. Shiels, M. Bäck, P. Stenvinkel, Inflammation and premature ageing in chronic kidney disease, Toxins (Basel) 12 (2020) 227, https://doi.org/10.3390/toxins12040227.
[57] J.-P. Coppé, P.-Y. Desprez, A. Krtolica, J. Campisi, The senescence-associated secretory phenotype: the dark side of tumor suppression, Annu. Rev. Pathol.: Mech. Dis. 5 (2010) 99–118, https://doi.org/10.1146/annurev-pathol-121808-102144.
[58] D. Saul, R.L. Kosinsky, E.J. Atkinson, M.L. Doolittle, X. Zhang, N.K. LeBrasseur, R. J. Pignolo, P.D. Robbins, L.J. Niedernhofer, Y. Ikeno, D. Jurk, J.F. Passos, L. J. Hickson, A. Xue, D.G. Monroe, T. Tchkonia, J.L. Kirkland, J.N. Farr, S. Khosla, A new gene set identifies senescent cells and predicts senescence-associated pathways across tissues, Nat. Commun. 13 (2022) 4827, https://doi.org/10.1038/s41467-022-32552-1.
[59] R. Masereeuw, H.A.M. Mutsaers, T. Toyohara, T. Abe, S. Jhawar, D.H. Sweet, J. Lowenstein, The kidney and uremic toxin removal: glomerulus or tubule? Semin. Nephrol. 34 (2014) 191–208, https://doi.org/10.1016/j.semnephrol.2014.02.010.
[60] H. Miao, Y. Wang, X. Yu, L. Zou, Y. Guo, W. Su, F. Liu, G. Cao, Y. Zhao, Lactobacillus species ameliorate membranous nephropathy through inhibiting the aryl hydrocarbon receptor pathway via tryptophan-produced indole metabolites, Br. J. Pharmacol. (2023), https://doi.org/10.1111/bph.16219.
[61] Y. Li, C. Zhou, W. Lei, K. Wang, J. Zheng, Roles of aryl hydrocarbon receptor in endothelial angiogenic responses†, Biol. Reprod. 103 (2020) 927–937, https://doi.org/10.1093/biolre/ioaa128.
[62] E. Hamza, L. Metzinger, V. Metzinger-Le Meuth, Uremic toxins affect erythropoiesis during the course of chronic kidney disease: a review, Cells 9 (2020) 2039, https://doi.org/10.3390/cells9092039.
[63] E. Hamza, M. Vallejo-Mudarra, H. Ouled-Haddou, C. García-Caballero, M. Guerrero-Hue, L. Santier, S. Rayego-Mateos, I.A. Larabi, J.-C. Alvarez, L. Garçon, Z.A. Massy, G. Choukroun, J.A. Moreno, L. Metzinger, V. Metzinger-Le Meuth, Indoxyl sulfate impairs erythropoiesis at BFU-E stage in chronic kidney disease, Cell. Signal. 104 (2023) 110583, https://doi.org/10.1016/j.cellsig.2022.110583.
[64] A. Al Halawani, S.M. Mithieux, G.C. Yeo, E. Hosseini-Beheshti, A.S. Weiss, Extracellular vesicles: interplay with the extracellular matrix and modulated cell responses, Int. J. Mol. Sci. 23 (2022) 3389, https://doi.org/10.3390/ijms23063389.
[65] S. Lewin, S. Hunt, D.W. Lambert, Extracellular vesicles and the extracellular matrix: a new paradigm or old news? Biochem. Soc. Trans. 48 (2020) 2335–2345, https://doi.org/10.1042/BST20200717.
[66] K. Rilla, A.-M. Mustonen, U.T. Arasu, K. Härkönen, J. Matilainen, P. Nieminen, Extracellular vesicles are integral and functional components of the extracellular matrix, Matrix Biol. 75–76 (2019) 201–219, https://doi.org/10.1016/j.matbio.2017.10.003.
[67] A. Sabatino, L. Cuppari, P. Stenvinkel, B. Lindholm, C.M. Avesani, Sarcopenia in chronic kidney disease: what have we learned so far? J. Nephrol. 34 (2021) 1347–1372, https://doi.org/10.1007/s40620-020-00840-y.
[68] M. Fontaine, S. Herkenne, O. Ek, A. Paquot, A. Boeckx, C. Paques, O. Nivelles, M. Thiry, I. Struman, Extracellular vesicles mediate communication between endothelial and vascular smooth muscle cells, Int. J. Mol. Sci. 23 (2021) 331, https://doi.org/10.3390/ijms23010331.
[69] D.W. Hagey, M. Ojansivu, B.R. Bostancioglu, O. Saher, J.P. Bost, M.O. Gustafsson, R. Gramignoli, M. Svahn, D. Gupta, M.M. Stevens, A. Görgens, S. EL Andaloussi, The cellular response to extracellular vesicles is dependent on their cell source and dose, Sci. Adv. 9 (2023), https://doi.org/10.1126/sciadv.adh1168.
[70] A. Carmona, F. Guerrero, P. Buendia, T. Obrero, P. Aljama, J. Carracedo, Microvesicles derived from indoxyl sulfate treated endothelial cells induce endothelial progenitor cells dysfunction, Front. Physiol. 8 (2017), https://doi.org/10.3389/fphys.2017.00666.
[71] C. Diorio, R. Shraim, L.A. Vella, J.R. Giles, A.E. Baxter, D.A. Oldridge, S.W. Canna, S.E. Henrickson, K.O. McNerney, F. Balamuth, C. Burudpakdee, J. Lee, T. Leng, A. Farrel, M.P. Lambert, K.E. Sullivan, E.J. Wherry, D.T. Teachey, H. Bassiri, E. M. Behrens, Proteomic profiling of MIS-C patients indicates heterogeneity relating to interferon gamma dysregulation and vascular endothelial dysfunction, Nat. Commun. 12 (2021) 7222, https://doi.org/10.1038/s41467-021-27544-6.
[72] T. Feldreich, C. Nowak, T. Fall, A.C. Carlsson, J.-J. Carrero, J. Ripsweden, A. R. Qureshi, O. Heimbürger, P. Barany, P. Stenvinkel, N. Vuilleumier, P.A. Kalra, D. Green, J. Ärnlöv, Circulating proteins as predictors of cardiovascular mortality in end-stage renal disease, J. Nephrol. 32 (2019) 111–119, https://doi.org/10.1007/s40620-018-0556-5.
[73] C. Yu, Y. Wan, W. Xu, X. Jin, S. Zhang, M. Xin, H. Jiang, X. Cheng, Increased circulating cathepsin L in patients with coronary artery disease, Int. Heart J. 62 (2021) 9–15, https://doi.org/10.1536/ihj.20-182.
[74] Y. Cao, X. Liu, Y. Li, Y. Lu, H. Zhong, W. Jiang, A.F. Chen, T.R. Billiar, H. Yuan, J. Cai, Cathepsin L activity correlates with proteinuria in chronic kidney disease in humans, Int. Urol. Nephrol. 49 (2017) 1409–1417, https://doi.org/10.1007/s11255-017-1626-7.
[75] A. En, Y. Takauji, D. Ayusawa, M. Fujii, The role of lamin B receptor in the regulation of senescence-associated secretory phenotype (SASP), Exp. Cell Res. 390 (2020) 111927, https://doi.org/10.1016/j.yexcr.2020.111927.
[76] T. Djuric, J. Kuveljic, A. Djordjevic, M. Dekleva, G. Stankovic, A. Stankovic, M. Zivkovic, Association of *MMP1* and *MMP3* haplotypes with myocardial infarction and echocardiographic parameters of the left ventricle, Mol. Genet. Genomic Med. 10 (2022), https://doi.org/10.1002/mgg3.2022.